Allosteric Interactions between the Nucleotide-Binding Sites and the ssDNA-Binding Site in the PriA Helicase−ssDNA Complex. 3†

Aaron L. Lucius, Maria J. Jezewska, and Wlodzimierz Bujalowski*

Department of Biochemistry and Molecular Biology, Department of Obstetrics and Gynecology, the Sealy Center for Structural Biology, Sealy Center for Cancer Cell Biology, The University of Texas Medical Branch at Galveston, 301 University Boulevard, Galveston, Texas 77555-1053

Received September 9, 2005; Revised Manuscript Received March 8, 2006

ABSTRACT: Allosteric interactions between the strong and weak nucleotide-binding sites and the total and proper single-stranded (ss)DNA-binding sites of the *Escherichia coli* PriA helicase have been analyzed using the fluorescence titration technique. Binding of the DNA exclusively to the proper DNA-binding site of the helicase, profoundly affects the intrinsic affinities of both nucleotide-binding sites, indicating a direct communication between the nucleotide-binding sites and the proper DNA-binding site. The communication involves conformational changes of the entire protein molecule. Nevertheless, the bound DNA differently affects the structures of the strong and weak nucleotide-binding sites. While the polarity of the strong site is moderately diminished, the polarity of the weak site is dramatically increased, indicating an intimate involvement of the weak site in controlling the helicase interactions with the DNA. The strong site does not directly control the DNA affinity of the enzyme. Only when the helicase has both nucleotide-binding sites saturated with ADP but not with ATP analogues does the enzyme have an increased affinity for the ssDNA, indicating that the control of ssDNA affinity involves a coordinated action of both nucleotide-binding sites and depends upon the phosphate group of the bound cofactor. A dramatic increase of the DNA affinity, when the DNA encompasses the total DNA-binding site of the enzyme, with both nucleotide-binding sites saturated with ADP or NDP, indicates that an additional area of the protein within the total DNA-binding site becomes engaged in interactions with the DNA. The significance of these results for the enzyme activities in the DNA unwinding and recognition is discussed.

Major processes of DNA and RNA metabolism, such as replication, recombination, repair, and translation, require that the duplex regions of the nucleic acid be unwound to form transiently a metabolically active single-stranded (ss)DNA intermediate (*1*−*7*). This reaction is catalyzed by a class of enzymes called helicases and is fueled by the hydrolysis of nucleotide triphosphates (*1*−*5*). The PriA helicase is a DNA replication enzyme in the *Escherichia coli* cell that is involved in DNA replication, recombination, and repair processes (*8*−*14*). The protein plays a key role in the ordered assembly of the primosome, as well as in propelling the mechanical translocation of the primosome machine along the DNA lattice. The enzyme has also been recognized as the factor that initiates the restarting of the stalled replication fork at the damaged DNA sites (*14*−*16*). On the basis of the primary structure, the PriA protein is classified as a member of the SF2 superfamily of helicases (*17*).

Equilibrium thermodynamic and stopped-flow kinetic studies, described in companion papers (*46*, *47*), have shown that the PriA helicase has two nucleotide-binding sites, which dramatically differ in their affinities and structural and dynamic properties. The affinity of the strong site profoundly depends upon the structure of the phosphate group of the ATP cofactor and is controlled by Mg^{2+} binding to the cofactor and to the protein. In contrast, the weak nucleotide-binding site shows very modest base specificity. Its affinity is minimally affected by the structure of the phosphate group of the ATP cofactor and by the presence of Mg^{2+} cations. Nevertheless, the revealed presence of cooperative interactions between the bound cofactors provides evidence for the communication between the two nucleotide-binding sites (*46*).

Both nucleotide-binding sites also differ in their dynamic properties. Binding of the ADP analogue, 2′(3′)-*O*-(2,4,6-trinitrophenyl)adenosine 5′-diphosphate (TNP-ADP),[1] to the strong nucleotide-binding site is a minimum four-step sequential reaction, while the association of the ATP analogue with the same site proceeds through a three-step sequential mechanism (*47*). Unlike 2′(3′)-*O*-(2,4,6-trinitrophenyl)adenosine 5′-triphosphate (TNP-ATP), the ADP analogue passes through an intermediate, where it leaves the hydrophobic cleft of the site, thus, corroborating with the notion that the strong site is the high-affinity ATPase site of the enzyme (*47*). Contrary to the strong site, association of

† This work was supported by NIH Grant GM-46679 (to W.B.). A.L.L. was partially supported by J. B. Kempner fellowship.

* Corresponding author. Tel.: (409)772-5634. Fax: (409)772-1790. E-mail.: wbujalow@utmb.edu.

[1] Abbreviations: TNP-ATP, 2′(3′)-*O*-(2,4,6-trinitrophenyl)adenosine 5′-triphosphate; TNP-ADP, 2′(3′)-*O*-(2,4,6-trinitrophenyl)adenosine 5′-diphosphate; NTP, ribonucleoside 5′-triphosphate; NDP, ribonucleoside 5′-diphosphate; dNTP, deoxyribonucleoside 5′-triphosphate; dNDP, deoxyribonucleoside 5′-diphosphate; PAS, primosome assembly site; EDTA, ethylenediaminetetraacetic acid disodium salt.

10.1021/bi0518287 CCC: $33.50
Published on Web 05/20/2006

the ADP analogue with the weak site proceeds in a simpler two-step sequential mechanism, while ATP analogue binding is still characterized by three steps. The different dynamics of the ADP analogue in the weak nucleotide-binding site, as compared to the ATP analogue, suggests a different function of the nucleoside di- and triphosphates bound to the weak site (*47*).

Recall, the total DNA-binding site of the PriA helicase occludes 20 ± 3 nucleotides (*18*−*20*). However, the enzyme has a proper ssDNA-binding site, within the total DNA-binding site, which can efficiently engage in interactions with only ~6−8 nucleotide residues, significantly less than the total DNA-binding site. The proper DNA-binding site is located in the central part of the enzyme molecule, on a structurally separated domain, with the protein matrix protruding on both sides of the proper site (*18*−*20*). Such a location of the proper DNA-binding site allows the enzyme to efficiently search and recognize small patches of ssDNA; i.e., it is an active, ssDNA gap-searching site of the helicase (*20*). In the course of the unwinding reaction of the duplex DNA, the affinity of a helicase for the DNA changes under the control of the nucleotide binding and/or hydrolysis (*2*−*4*). Therefore, examination of the effect of the nucleotide cofactors, bound to the strong and weak nucleotide-binding sites, on the helicase interactions with the ssDNA in the proper and total DNA-binding sites is of fundamental importance for elucidation of the mechanism of the enzyme functioning in replication and recombination processes (*2*−*4*).

In this paper, we report quantitative analyses of the effect of the nucleotide cofactors bound to the strong and weak nucleotide-binding sites of the PriA helicase on the interactions of the enzyme with the ssDNA, which can bind exclusively to the proper DNA-binding site or can encompass the entire total DNA-binding site of the helicase. The data indicate a direct communication between the nucleotide-binding sites and the proper DNA-binding site that involves conformational changes of the entire protein molecule. However, the strong site does not directly control the DNA affinity of the enzyme. Such control involves a coordinated action of both nucleotide-binding sites and depends upon the structure of the phosphate group of the bound cofactor. A dramatic increase of the DNA affinity with both nucleotide-binding sites saturated with ADP or ribonucleoside 5′-diphosphate (NDP) indicates that an additional area of the protein, within the total DNA-binding site, become engaged in interactions with the nucleic acid.

MATERIALS AND METHODS

Reagents and Buffers. All chemicals were reagent-grade. All solutions were made as described in the companion paper (*46*). The NaCl and $MgCl_2$ concentrations in the buffer are indicated in the text (*46*, *47*). The *E. coli* PriA protein has been isolated and purified as previously described (*18*, *19*, *46*).

Nucleotide and Nucleic Acids. TNP-ATP and TNP-ADP were from Molecular Probes (Eugene, OR) (*32*). ATP was from CalBiochem, and ADP, dADP, GDP, and TDP were from Sigma (St. Louis, MO). Nucleotides used in the binding studies were >95% pure as judged by TLC on silica. All ssDNA oligomers were purchased from Midland Certified Reagents (Midland, TX). The etheno derivative, $d\epsilon A(p\epsilon A)_9$ and $d\epsilon A(p\epsilon A)_{19}$, of $dA(pA)_9$ and $dA(pA)_{19}$ were obtained by modification with chloroacetaldehyde (*21*−*24*). Concentrations of all ssDNA oligomers have been spectrophotometrically determined as described previously by us (*18*−*22*).

Fluorescence Measurements. All steady-state fluorescence titrations were performed using the Fluorolog F-11 (Spex Jobin Yvon) as described previously and in companion papers (*18*, *19*, *25*−*27*, *46*, *47*). Binding of the PriA helicase to etheno derivatives of the ssDNA oligomers, $d\epsilon A(p\epsilon A)_9$ and $d\epsilon A(p\epsilon A)_{19}$, was followed by monitoring the fluorescence of the etheno derivatives of the nucleic acids (λ_{ex} = 325 nm, λ_{em} = 410 nm) (*18*, *19*, *25*−*27*). The relative increase of fluorescence, ΔF_{obs}, of the cofactor or ssDNA emission upon binding to the PriA helicase is defined as $\Delta F_{obs} = (F_o - F_i)/F_o$, where F_i is the fluorescence of a TNP analogue or ssDNA oligomer at a given titration point and F_o is the initial value of the fluorescence of the sample (*18*, *19*, *25*−*29*).

Stopped-Flow Kinetics. All fluorescence stopped-flow kinetics experiments were performed using the SX.18MV stopped-flow instrument (Applied Photophysics, Leatherhead, U.K.) as described before in ref *20*. The reactions were monitored following the total fluorescence emission of the etheno derivatives of the ssDNAs, with λ_{ex} = 325 nm, and the emission was monitored through the GG400 cutoff filter (Schott, PA).

RESULTS

Binding of the ADP and ATP Analogues, TNP-ADP and TNP-ATP, to the PriA Helicase Associated with the ssDNA in the Proper and Total DNA-Binding Sites, Monitored by the Fluorescence Emission of the Enzyme. The PriA helicase can bind the ssDNA with significant affinity in the absence of the nucleotide cofactors (*18*−*20*). In the first set of experiments, we have utilized this fact to examine the effect of the ssDNA associated with the enzyme on the binding of nucleotide analogues, TNP-ATP and TNP-ADP, to the strong and weak nucleotide-binding sites of the helicase. Association of these analogues with the PriA helicase is accompanied by the quenching of the protein fluorescence, which is different and characteristic for the strong and weak nucleotide-binding sites (*46*). The experiments were performed in the absence of magnesium to avoid precipitation of the protein−nucleic acid complex at higher nucleotide concentrations (*18*, *19*, *46*).

Fluorescence titration of the PriA−$dA(pA)_9$ complex, with TNP-ADP in buffer C (pH 7.0, 20 °C), containing 20 mM NaCl and 0.1 mM ethylenediaminetetraacetic acid disodium salt (EDTA), is shown in Figure 1. For a comparison, the titration of the helicase in the same solution conditions in the absence of the ssDNA 10-mer is also included (*46*). Recall, the ssDNA 10-mer exclusively binds to the proper DNA-binding site of the PriA helicase (*18*−*20*). At the applied ssDNA oligomer concentration, the population of the protein molecules is predominantly in the complex with the nucleic acid (*18*−*20*). The analysis of the titration curves has been performed as described in a companion paper (*46*). The solid lines in Figure 1 are nonlinear least-squares fits of the titration curves using the statistical thermodynamic

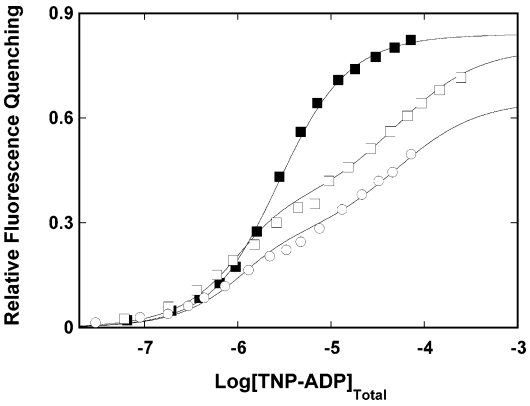

FIGURE 1: Fluorescence titration of PriA helicase with TNP-ADP in buffer C (pH 7.0, 20 °C), containing 20 mM NaCl and 0.1 mM EDTA, in the absence (■) and presence (□) of the ssDNA 10-mer, $dA(pA)_9$, or (○) the presence of the ssDNA 20-mer, $dA(pA)_{19}$. The concentrations of the enzyme and nucleic acids are 1.0×10^{-6} and 3×10^{-5} M, respectively. The solid lines are nonlinear least-squares fits of the titration curves, according to the model of two different, discrete, and cooperative binding sites (*46*) using a single set of binding parameters: $K_{B_1} = 5.1 \times 10^7$ M^{-1}, $K_{B_2} = 3.7 \times 10^5$ M^{-1}, $\sigma = 1$, $\Delta F_1 = 0.2$, and $\Delta F_2 = 0.64$, in the absence of the ssDNA 10- or 20-mer; $K_{B_1} = 2.5 \times 10^6$ M^{-1}, $K_{B_2} = 1.9 \times 10^4$ M^{-1}, $\sigma = 1$, $\Delta F_1 = 0.38$, and $\Delta F_2 = 0.42$, in the presence of the 10-mer; and $K_{B_1} = 2.0 \times 10^6$ M^{-1}, $K_{B_2} = 1.9 \times 10^4$ M^{-1}, $\sigma = 1$, $\Delta F_1 = 0.28$, and $\Delta F_2 = 0.37$, in the presence of the ssDNA 20-mer.

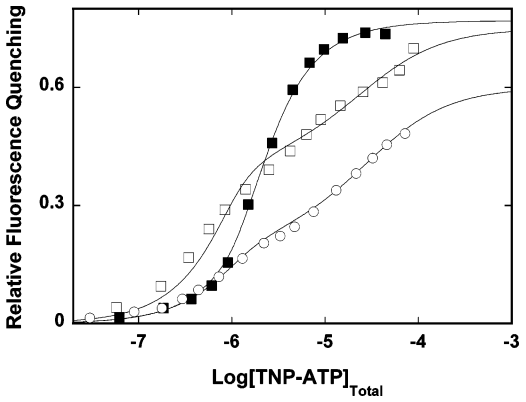

FIGURE 2: Fluorescence titration of PriA helicase with TNP-ATP in buffer C (pH 7.0, 20 °C), containing 20 mM NaCl and 0.1 mM EDTA, in the absence (■) and presence (□) of the ssDNA 10-mer, $dA(pA)_9$, or (○) in the presence of the ssDNA 20-mer, $dA(pA)_{19}$. The concentrations of the enzyme and nucleic acids are 1.0×10^{-6} and 3×10^{-5} M, respectively. The solid lines are nonlinear least-squares fits of the titration curves, according to the model of two different, discrete, and cooperative binding sites (*46*) using a single set of binding parameters: $K_{B_1} = 1 \times 10^8$ M^{-1}, $K_{B_2} = 7.8 \times 10^5$ M^{-1}, $\sigma = 1$, $\Delta F_1 = 0.18$, and $\Delta F_2 = 0.59$, in the absence of the ssDNA 10- or 20-mer; $K_{B_1} = 7.5 \times 10^6$ M^{-1}, $K_{B_2} = 4.0 \times 10^4$ M^{-1}, $\sigma = 1$, $\Delta F_1 = 0.44$, and $\Delta F_2 = 0.31$, in the presence of the 10-mer; and $K_{B_1} = 3.5 \times 10^6$ M^{-1}, $K_{B_2} = 3.4 \times 10^4$ M^{-1}, $\sigma = 1$, $\Delta F_1 = 0.24$, and $\Delta F_2 = 0.42$, in the presence of the ssDNA 20-mer.

model of two discrete binding sites with cooperative interactions between the sites (eqs 4−6 of ref *46*).

The effect of the nucleic acid on the binding of the nucleotide analogue to both nucleotide-binding sites, in the examined solution conditions, is dramatic, although the ssDNA 10-mer encompasses only the proper DNA-binding site of the enzyme (*18*−*20*). The intrinsic affinities of both the strong and weak nucleotide-binding sites are strongly decreased by a factor of ∼20 and ∼18, respectively. However, the fluorescence quenching accompanying the binding to the strong site is increased from $\Delta F_1 \sim 0.2$ to ∼0.38, while the analogous parameter for the weak binding site is decreased from $\Delta F_2 \sim 0.64$ to ∼0.42, indicating a different effect of the nucleic acid on the structure of the strong binding site, as compared to the weak nucleotide-binding site (see below and the Discussion). As a result of the induced changes in both the intrinsic affinities and spectroscopic parameters, the presence of two binding phases, corresponding to the association of the nucleotide cofactor with the strong and weak nucleotide-binding sites, becomes very prominent for the protein complex with the nucleic acid (*46*).

The ssDNA 20-mer encompasses the total DNA-binding site of the helicase, which has the site size of 20 ± 3 nucleotide residues (*18*−*20*). Fluorescence titration of the PriA−ssDNA 20-mer [$dA(pA)_{19}$] complex with TNP-ADP is included in Figure 1. The presence of the 20-mer has a similar effect on the intrinsic affinities for both nucleotide-binding sites, as observed for the 10-mer, with K_{B_1} and K_{B_2} decreased by a factor of ∼25 and ∼18, respectively, as compared to the same parameters obtained in the absence of DNA (Figure 1). Nevertheless, although the affinities are affected in a similar way by the 10- and 20-mer, the changes of the fluorescence quenching, induced by the 20-mer, are different, as compared to the changes induced by the 10-mer, with $\Delta F_1 = 0.28 \pm 0.03$ and $\Delta F_2 = 0.37 \pm 0.05$.

Analogous fluorescence titrations of the PriA−ssDNA 10-mer and the PriA−ssDNA 20-mer complexes, with the ATP analogue, TNP-ATP, in buffer C (pH 7.0, 20 °C), containing 20 mM NaCl and 0.1 mM EDTA, together with the titration performed in the absence of the nucleic acids is shown in Figure 2. Saturation of the proper DNA-binding site with the ssDNA 10-mer decreases the values of K_{B_1} and K_{B_2} for the ATP analogue by a factor of ∼14 and ∼19, respectively, with respect to the same parameters obtained in the absence of DNA, although a more pronounced decrease of the affinities is obtained for the ssDNA 20-mer, where the corresponding factors are ∼27 and ∼22. As observed for the ADP analogue (Figure 1), the significant difference between the effect of the 10- and 20-mer on the binding of the ATP analogue occurs in values of the quenching parameters, where, in the presence of the 10-mer, $\Delta F_1 = 0.44 \pm 0.03$ and $\Delta F_2 = 0.31 \pm 0.05$, while the same parameters are ∼0.18 and ∼0.59, respectively, in the absence of the nucleic acid (Figure 2). In the case of the 20-mer, the induced changes of the quenching parameters are less pronounced, as also observed for the ADP analogue (parts a and b of Figure 1), with $\Delta F_1 = 0.24 \pm 0.03$ and $\Delta F_2 = 0.32 \pm 0.05$. It is evident that the ssDNA, whether bound to the proper ssDNA-binding site or encompassing the total ssDNA-binding site, has a similar effect on the binding affinities of the ADP and ATP analogues to the strong and weak nucleotide-binding sites of the PriA helicase, although the effects of the 10- and 20-mer on the structure of both nucleotide-binding sites are different. Nevertheless, the similarity between the effects of the 10- and 20-mer on the binding of the ADP and ATP analogues indicates that the induced energetic and structural changes of the strong and weak nucleotide-binding sites are an intrinsic property of the protein−DNA complex independent of the number of phosphate groups of the nucleotide cofactor (see the Discussion).

Binding of the Nucleotide Analogues, TNP-ADP and TNP-ATP, to the PriA Helicase Associated with the ssDNA in the Proper and Total DNA-Binding Sites, Monitored by the Fluorescence Emission of the Analogues. In the studies described in the previous section, the effect of the nucleic acid on nucleotide binding to the strong and weak nucleotide-binding sites of the PriA helicase has been performed by monitoring the quenching of the protein fluorescence. Thus, the binding process was monitored by examining the spectroscopic signal originating from the side of the protein. However, as pointed out in ref *47*, binding of the TNP analogues to the PriA helicase results in a very large increase of the cofactor fluorescence. Moreover, the emission of the TNP moiety is very sensitive to the polarity of the environment of the binding site (*30*−*33*). Therefore, to obtain further insight about the nature of the conformational changes in the strong and weak nucleotide-binding sites of the PriA helicase, induced by the nucleic acid, we examined the binding of the TNP-ADP and TNP-ATP to the PriA−ssDNA complexes, by monitoring the nucleotide cofactor fluorescence (*47*).

Fluorescence titrations of TNP-ADP with PriA helicase in buffer C (pH 7.0, 20 °C), containing 20 mM NaCl, 0.1 mM EDTA, and 3×10^{-5} M ssDNA 10-mer, $dA(pA)_9$, at three different concentrations of the cofactor, are shown in Figure 3a. The selected concentration of the ssDNA oligomer ensures that the protein is saturated with the DNA over the entire range of the protein concentration applied in the titrations (*18*−*20*). As previously discussed, the titration at the highest concentration of the cofactor (7×10^{-5} M) could only be performed over a limited protein concentration range, because of the precipitation of the complex at high protein and nucleotide concentrations (*46*, *47*). At higher cofactor concentrations, a given relative fluorescence increase, ΔF_{obs}, is reached at a higher concentration of the protein−ssDNA complex, because more protein is required to saturate the cofactor (*25*−*29*).

Analyses of the titration curves in Figure 3a have been performed in the same way as described in ref *47*, using two derived parametric equations, which analytically describe the titration curves. Briefly, we know the statistical thermodynamic model that describes the observed binding process and the values of all binding parameters in the model (Figure 1). Thus, there are two distinct nucleotide-binding sites on the enzyme characterized by the intrinsic binding constants, K_{B_1} and K_{B_2}, and the cooperativity parameter, σ, for TNP-ADP (*46*, *47*). The total partition function, Z, and the total average degree of binding, $\sum\Theta_i$, of the considered system are (*47*)

$$Z = 1 + (K_{B_1} + K_{B_2})L_F + K_{B_1}K_{B_2}\sigma L_F^2 \qquad (1)$$

and

$$\sum\Theta_i = \frac{(K_{B_1} + K_{B_2})L_F + 2K_{B_1}K_{B_2}\sigma L_F^2}{Z} \qquad (2)$$

The total nucleotide cofactor concentration, L_T, is related to its free concentration by the mass conservation equation

$$L_T = L_F[1 + (K_{B_1} + K_{B_2})P_F] + 2K_{B_1}K_{B_2}\sigma L_F^2 P_F \qquad (3)$$

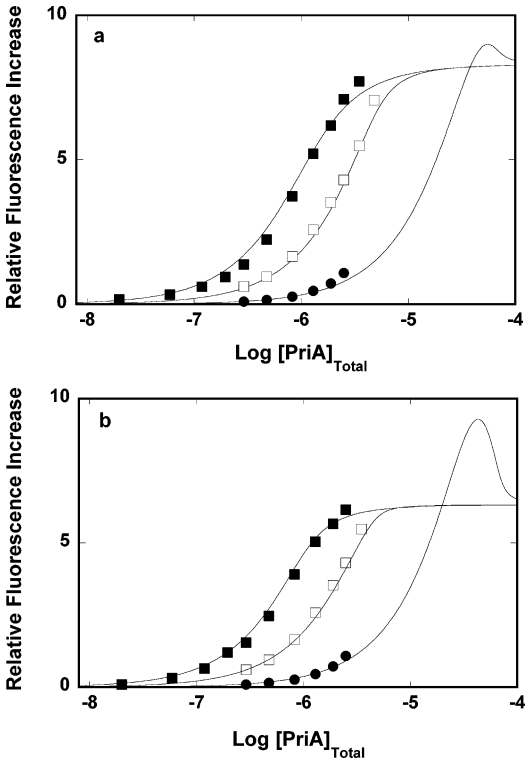

FIGURE 3: (a) Fluorescence titration of TNP-ADP with the PriA helicase, in buffer C (pH 7.0, 20 °C), containing 20 mM NaCl and 0.1 mM EDTA, in the presence of 3×10^{-5} M ssDNA 10-mer, $dA(pA)_9$, at three different TNP-ATP concentrations: (■) 1.0×10^{-6} M, (□) 5.0×10^{-6} M, and (●) 7.0×10^{-5} M. The solid lines are nonlinear least-squares fits of the titration curves, using eqs 2−6, with a single set of binding and spectroscopic parameters: $K_{B_1} = 2.5 \times 10^6$ M^{-1}, $K_{B_2} = 1.9 \times 10^4$ M^{-1}, $\sigma = 1$, $\Delta F_{1_{max}} = 8.3$, and $\Delta F_{2_{max}} = 8.0$. (b) Fluorescence titration of TNP-ATP with the PriA helicase, in buffer C (pH 7.0, 20 °C), containing 20 mM NaCl and 0.1 mM EDTA, in the presence of 3×10^{-5} M ssDNA 10-mer, $dA(pA)_9$, at three different TNP-ATP concentrations: (■) 1.0×10^{-6} M, (□) 5.0×10^{-6} M, and (●) 7.0×10^{-5} M. The solid lines are nonlinear least-squares fits of the titration curves, using eqs 2−6, with a single set of binding and spectroscopic parameters: $K_{B_1} = 7.5 \times 10^6$ M^{-1}, $K_{B_2} = 4.0 \times 10^4$ M^{-1}, $\sigma = 1$, $\Delta F_{1_{max}} = 6.3$, and $\Delta F_{2_{max}} = 10.0$.

where P_F is the free concentration of the PriA protein. The solution of eq 3 provides the first analytical parametric equation for the free nucleotide cofactor concentration, L_F, as a function of P_F and L_T, which is

$$L_F = \left(-(1 + K_{B_1} + K_{B_2})P_F + \sqrt{[1 + (K_{B_1} + K_{B_2})P_F{}^2 + 8K_{B_1}K_{B_2}\sigma L_T P_F}\right) \Big/ 4K_{B_1}K_{B_2}\sigma P_F \qquad (4)$$

The second parametric equation is the expression for the total protein concentration, P_T, as a function of the free protein concentration, P_F, i.e.,

$$P_T = P_F[(1 + K_{B_2})L_F + K_{B_1}K_{B_2}\sigma L_F^2] \qquad (5)$$

The observed relative fluorescence increase, ΔF_{obs}, of the nucleotide analogue, in the presence of the helicase, is then described by

$$\Delta F_{obs} = \Delta F_{1_{max}}\left(\frac{K_{B_1} L_F P_F}{L_T}\right) + \Delta F_{2_{max}}\left(\frac{K_{B_2} L_F P_F}{L_T}\right) + (\Delta F_{1_{max}} + \Delta F_{2_{max}})\left(\frac{K_{B_1} K_{B_2} \sigma L_F^2 P_F}{L_T}\right) \quad (6)$$

where L_T is defined by eq 3. The parameters, $\Delta F_{1_{max}}$ and $\Delta F_{2_{max}}$ are the relative molar fluorescence increases of the nucleotide cofactor emission bound to the strong and weak nucleotide-binding sites, respectively (*47*).

Binding of TNP-ADP to the strong and weak nucleotide-binding site of the PriA helicase is characterized by $K_{B_1} = (2.5 \pm 0.5) \times 10^6$ M^{-1}, $K_{B_2} = (1.9 \pm 0.6) \times 10^4$ M^{-1}, and $\sigma = 1 \pm 0.3$, determined independently, using the quenching of the protein fluorescence to monitor the binding (Figure 1). The solid lines in Figure 3a are nonlinear least-squares fits of the experimental titration curves, using eq 6, with the above values of the binding parameters and only two fitting parameters, $\Delta F_{1_{max}}$ and $\Delta F_{2_{max}}$, which provide $\Delta F_{1_{max}} = 8.3 \pm 0.3$ and $\Delta F_{2_{max}} = 8.0 \pm 2$, respectively. The values of the same molar fluorescence increases accompanying the binding of the ADP analogue binding to the strong and weak nucleotide-binding site of the PriA helicase, obtained in the absence of the nucleic acid, are $\Delta F_{1_{max}} = 12.0 \pm 0.3$ and $\Delta F_{2_{max}} = 0.3 \pm 0.1$ (*47*). Thus, in the presence of the ssDNA 10-mer, the value of $\Delta F_{1_{max}}$ is decreased by ~30%. However, the effect of the nucleic acid on $\Delta F_{2_{max}}$ is dramatic, with the value of the parameter increased by a factor of ~27 (see the Discussion).

Analogous fluorescence titrations of the ATP analogue, TNP-ATP, with PriA helicase in buffer C (pH 7.0, 20 °C), containing 20 mM NaCl, 0.1 mM EDTA, and 3×10^{-5} M ssDNA 10-mer, dA(pA)$_9$, at three different concentrations of the cofactor, are shown in Figure 3b. The solid lines in Figure 3b are nonlinear least-squares fits of the experimental titration curves, using eq 6, with only two fitting parameters, $\Delta F_{1_{max}}$ and $\Delta F_{2_{max}}$, and with $K_{B_1} = (7.5 \pm 0.5) \times 10^6$ M^{-1}, $K_{B_2} = (4.0 \pm 0.6) \times 10^4$ M^{-1}, and $\sigma = 1 \pm 0.3$, determined independently using protein fluorescence quenching to monitor the binding (Figure 2). The fit provides $\Delta F_{1_{max}} = 6.3 \pm 0.3$ and $\Delta F_{2_{max}} = 10.0 \pm 2.0$, respectively. The values of the same molar fluorescence increases accompanying the binding of the ATP analogue, obtained in the absence of the nucleic acid, are $\Delta F_{1_{max}} = 12.4 \pm 0.3$ and $\Delta F_{2_{max}} = 0.3 \pm 0.1$ (*47*). Thus, as observed for the ADP analogue, in the presence of the ssDNA 10-mer, the value of $\Delta F_{1_{max}}$ is significantly decreased, while the value of $\Delta F_{2_{max}}$ is dramatically increased. Clearly, the nucleic acid, bound to the proper DNA-binding site of the PriA helicase, profoundly affects the polarity of the environment of the bound nucleotide analogues in both nucleotide-binding sites, and the induced changes in the structure of both binding sites are independent of the number of phosphate groups of the cofactor (see the Discussion).

Association of the ssDNA 10- and 20-mer with the Proper and Total DNA-Binding Sites of the PriA Helicase in the Presence of ADP Bound to the Strong and Weak Nucleotide-Binding Sites of the Enzyme. Interactions of the PriA helicase with etheno derivatives of the homo-adenosine ssDNAs are accompanied by a strong fluorescence increase of the nucleic acid, which has previously allowed us to examine the energetics and kinetics of the helicase−ssDNA interactions (*18*−*20*). The effect of ADP bound in the strong nucleotide-binding site, as well as in both the strong and weak nucleotide-binding sites of the PriA helicase on the interactions of the enzyme with the ssDNA, bound in the proper DNA-binding site, has been examined using the ssDNA 10-mer, dϵA(pϵA)$_9$, which exclusively binds to the proper DNA-binding site (*18*−*20*). Correspondingly, the effect of ADP on the interactions within the total DNA-binding site has been addressed using the ssDNA 20-mer, dϵA(pϵA)$_{19}$, which encompasses the total DNA-binding site of the PriA helicase (*18*−*20*). Because substantial binding of ADP to the weak nucleotide-binding site requires high concentrations of the cofactor, the experiments have been performed at an elevated Mg^{2+} concentration to examine the interactions with the DNA at a high ADP concentration in the presence of saturating [Mg^{2+}].

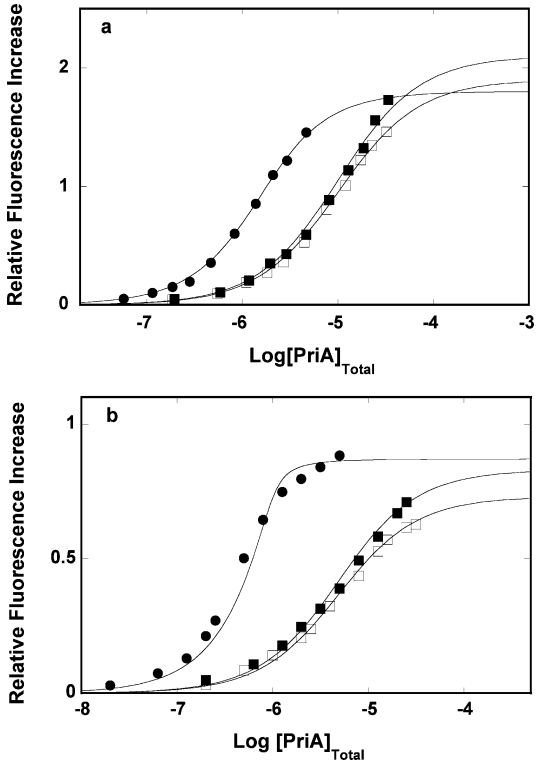

FIGURE 4: (a) Fluorescence titrations of the ssDNA 10-mer, dϵA(pϵA)$_9$, with the PriA helicase in buffer C (pH 7.0, 20 °C), containing 20 mM NaCl and 15 mM $MgCl_2$, in the absence and presence of different ADP concentrations: (■) 0 M, (□) 1×10^{-5} M, and (●) 5×10^{-3} M. The concentration of the ssDNA oligomer is 1×10^{-6} M. The solid lines are nonlinear least-squares fits of the titration curves, to the single-site binding isotherm (eq 7), using binding and spectroscopic parameters included in Table 1. (b) Fluorescence titrations of the ssDNA 20-mer, dϵA(pϵA)$_{19}$, with the PriA helicase in buffer C (pH 7.0, 20 °C), containing 20 mM NaCl and 15 mM $MgCl_2$, in the absence and presence of different ADP concentrations: (■) 0 M, (□) 1×10^{-5} M, and (●) 5×10^{-3} M. The concentration of the ssDNA oligomer is 1×10^{-6} M. The solid lines are nonlinear least-squares fits of the titration curves, to the single-site binding isotherm (eq 7), using binding and spectroscopic parameters included in Table 1.

Fluorescence titrations of the ssDNA 10-mer, dϵA(pϵA)$_9$, with the PriA helicase in buffer C (pH 7.0, 20 °C), containing 20 mM NaCl and 15 mM $MgCl_2$, in the absence and presence of ADP, at two different concentrations of the nucleotide cofactor, are shown in Figure 4a. Because of moderate affinity of the 10-mer and propensity of the protein−DNA

Table 1: Binding and Spectroscopic Parameters for the Association of the *E. coli* PriA Helicase with the ssDNA 10- and 20-mer, dϵA(pϵA)$_9$ and dϵA(pϵA)$_{19}$, in the Absence and Presence of ADP or ATPγS, with Cofactor Concentrations Saturating Only the Strong or Both the Strong and Weak Nucleotide-Binding Sites of the Helicase, in Buffer C (pH 7.0, 20 °C) Containing 20 mM NaCl and 15 mM $MgCl_2$

cofactor	K_{10} (M^{-1})	ΔF_{10}	K_{20} (M^{-1})	ΔF_{20}
none	$(1.1. \pm 0.3) \times 10^5$	2.1 ± 0.3	$(2.3 \pm 0.8) \times 10^5$	0.83 ± 0.15
[ADP] 1×10^{-5} M	$(1.1 \pm 0.3) \times 10^5$	1.9 ± 0.3	$(2.3 \pm 0.8) \times 10^5$	0.73 ± 0.15
[ADP] 5×10^{-3} M	$(1.0 \pm 0.3) \times 10^6$	1.8 ± 0.3	$(3.0 \pm 1.1) \times 10^7$	0.87 ± 0.15
[ATPγS] 1×10^{-4} M	$(9.0 \pm 2.8) \times 10^4$	2.0 ± 0.3	$(1.6 \pm 0.6) \times 10^5$	0.87 ± 0.15
[ATPγS] 5×10^{-3} M	$(5.7 \pm 1.9) \times 10^4$	1.8 ± 0.3	$(1.2 \pm 0.4) \times 10^5$	0.87 ± 0.15
[ADP], [ATPγS] 1.5×10^{-4} M, 5×10^{-3} M	$(9.0 \pm 2.8) \times 10^4$	1.3 ± 0.2	$(2.1 \pm 0.4) \times 10^5$	0.6 ± 0.12

complex to precipitate at high [ADP], the plateaus could not be reached in a single titration experiment. However, because these are simple 1:1 complexes of the enzyme and nucleic acids, determination of the inflection point of the titration curve provides sufficing information about the location of the plateau, because of the symmetry of the 1:1 isotherm (*34*). Nevertheless, the estimates of the relative maximum fluorescence increase, ΔF_{max}, were additionally obtained by directly adding the nucleic acid, in a series of very low concentrations, to a sample containing a high concentration of the helicase−ADP complex (data not shown) (*18*, *19*, *35*). The same approach has been used for all titrations discussed in this paper where the plateau could not be reached in a single titration experiment (see below). The solid lines in Figure 4a are nonlinear least-squares fits of the fluorescence titration curves, using the single-site binding isotherm (*18*, *19*)

$$\Delta F_{obs} = \Delta F_{max}\left(\frac{K_N P_F}{1 + K_N P_F}\right) \quad (7)$$

where K_N (in the considered case, $N = 10$) is the macroscopic binding constant of the ssDNA 10-mer and ΔF_{max} is the maximum relative fluorescence change of the nucleic acid at saturation. The obtained binding and spectroscopic parameters are included in Table 1. The presence of ADP exclusively in the strong nucleotide-binding site has a minimal, if any, effect on the 10-mer binding to the proper DNA-binding site, with ΔF_{max} being slightly lower in the presence of the cofactor (Figure 4a and Table 1). However, when ADP is bound to both the strong and weak nucleotide-binding sites, the affinity of the nucleic acid is increased by an order of magnitude with a concomitant further decrease of ΔF_{max}.

Fluorescence titrations of the ssDNA 20-mer, dϵA(pϵA)$_{19}$, with the PriA helicase in buffer C (pH 7.0, 20 °C), containing 20 mM NaCl and 15 mM $MgCl_2$, in the absence and presence of ADP, at two different concentrations of the nucleotide cofactor, are shown in Figure 4b. The solid lines in Figure 4b are nonlinear least-squares fits of the fluorescence titration curves, using a single-site binding isotherm as defined by eq 7. The obtained binding and spectroscopic parameters are included in Table 1. Similar to the ssDNA 10-mer (Figure 4a), binding of ADP to the strong nucleotide-binding site has a very minimal effect on the affinity of the ssDNA 20-mer for the total DNA-binding site, with the value ΔF_{max} being slightly lower in the presence of ADP. On the other hand, the presence of ADP in both the strong and weak nucleotide-binding sites has a dramatic effect on the nucleic acid binding. The affinity increases by a factor of ~130 as compared to only 1 order of magnitude increase observed for the 10-mer in the proper DNA-binding site (Table 1). Moreover, unlike the case of the 10-mer (Figure 4a), the value of ΔF_{max} is larger than ΔF_{max} obtained in the absence of ADP (Figure 4b) (see the Discussion).

Association of the ssDNA 10- and 20-mer, with the Proper and Total DNA-Binding Sites of the PriA Helicase in the Presence of the ATP Analogue, ATPγS, Bound to the Strong and Weak Nucleotide-Binding Sites of the Enzyme. Because PriA helicase is a potent ATPase in the presence of the ssDNA, the effect of the nucleoside triphosphate on the ssDNA binding to the enzyme has been performed in the presence of the ATP nonhydrolyzable analogue, ATPγS, which has the highest affinity, among all examined ATP analogues, for both the strong and weak nucleotide-binding sites of the enzyme (*46*). Fluorescence titrations of the ssDNA 10-mer, dϵA(pϵA)$_9$, with the PriA helicase in buffer C (pH 7.0, 20 °C), containing 20 mM NaCl and 15 mM $MgCl_2$, in the absence and presence of ATPγS, at two different concentrations of the nucleotide cofactor, are shown in Figure 5a. The estimates of the maximum fluorescence increase, ΔF_{max}, were obtained by directly adding the nucleic acid, at very low concentrations, to a sample containing a high concentration of the protein−ATPγS complex (see above). The solid lines in Figure 5a are nonlinear least-squares fits of the fluorescence titration curves, using a single-site binding isotherm defined by eq 7. The obtained binding and spectroscopic parameters are included in Table 1. The effect of the nucleoside triphosphate is very different from the effect observed in the case of ADP (parts a and b of Figure 4). Binding of ATPγS to the strong nucleotide-binding site slightly decreases the affinity of the 10-mer for the proper DNA-binding site of the helicase and the observed ΔF_{max} (Figure 5a and Table 1). However, binding of the ATP analogue to both the strong and weak nucleotide-binding sites, instead of strongly increasing the affinity, further decreases the value of the binding constant K_{10} and also ΔF_{max}.

A similar dramatic difference between the effect of ATPγS and ADP is observed in the case of the ssDNA 20-mer.

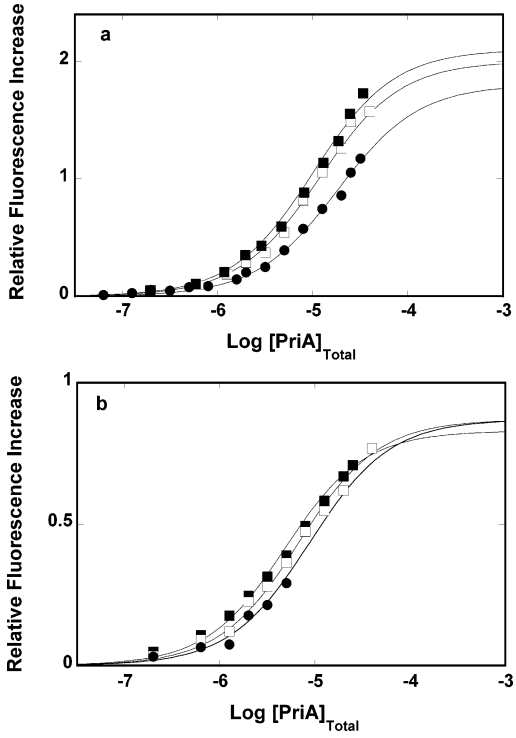

FIGURE 5: (a) Fluorescence titrations of the ssDNA 10-mer, dϵA-(pϵA)$_9$, with the PriA helicase in buffer C (pH 7.0, 20 °C), containing 20 mM NaCl and 15 mM $MgCl_2$, in the absence and presence of different ATPγS concentrations: (■) 0 M, (□) 5×10^{-4} M, and (●) 5×10^{-3} M. The concentration of the ssDNA oligomer is 1×10^{-6} M. The solid lines are nonlinear least-squares fits of the titration curves, to the single-site binding isotherm (eq 7), using binding and spectroscopic parameters included in Table 1. (b) Fluorescence titrations of the ssDNA 20-mer, dϵA(pϵA)$_{19}$, with the PriA helicase in buffer C (pH 7.0, 20 °C), containing 20 mM NaCl and 15 mM $MgCl_2$, in the absence and presence of different ATPγS concentrations: (■) 0 M, (□) 5×10^{-4} M, and (●) 5×10^{-3} M. The concentration of the ssDNA oligomer is 1×10^{-6} M. The solid lines are nonlinear least-squares fits of the titration curves, to the single-site binding isotherm (eq 7), using binding and spectroscopic parameters included in Table 1.

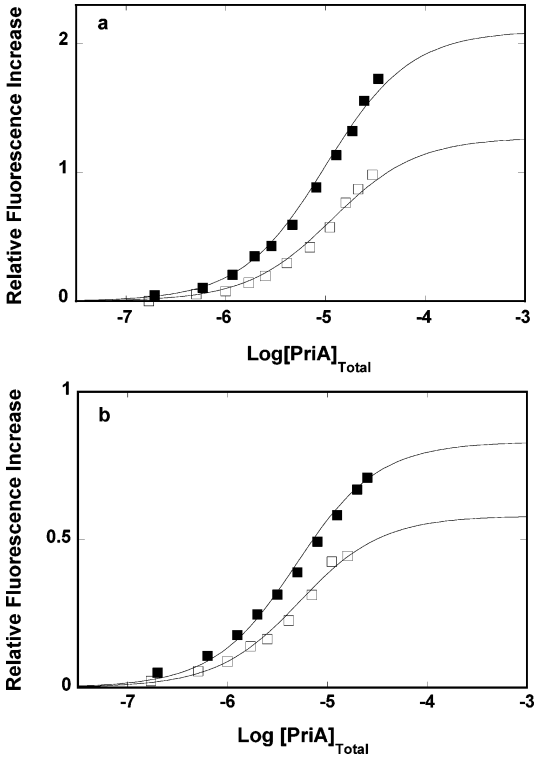

FIGURE 6: (a) Fluorescence titrations of the ssDNA 10-mer, dϵA-(pϵA)$_9$, with the PriA helicase in buffer C (pH 7.0, 20 °C), containing 20 mM NaCl and 15 mM $MgCl_2$, in the absence (■) and presence (□) of ADP and ATPγS at concentrations of 1.5×10^{-4} and 5×10^{-3} M, respectively. The concentration of the ssDNA oligomer is 1×10^{-6} M. The solid lines are nonlinear least-squares fits of the titration curves, to the single-site binding isotherm (eq 7), using binding and spectroscopic parameters included in Table 1. (b) Fluorescence titrations of the ssDNA 20-mer, dϵA(pϵA)$_{19}$, with the PriA helicase in buffer C (pH 7.0, 20 °C), containing 20 mM NaCl and 15 mM $MgCl_2$, in the absence (■) and presence (□) of ADP and ATPγS at concentrations of 1.5×10^{-4} and 5×10^{-3} M, respectively. The concentration of the ssDNA oligomer is 1×10^{-6} M. The solid lines are nonlinear least-squares fits of the titration curves, to the single-site binding isotherm (eq 7), using binding and spectroscopic parameters included in Table 1.

Fluorescence titrations of the ssDNA 20-mer, dϵA(pϵA)$_{19}$, with the PriA helicase in buffer C (pH 7.0, 20 °C), containing 20 mM NaCl and 15 mM $MgCl_2$, in the absence and presence of ATPγS, at two different concentrations of the nucleoside triphosphate, are shown in Figure 5b. The solid lines in Figure 5b are nonlinear least-squares fits of the fluorescence titration curves, using a single-site binding isotherm as defined by eq 7. The obtained binding and spectroscopic parameters are included in Table 1. Unlike the behavior observed in the case of ADP, binding of ATPγS exclusively to the strong nucleotide-binding site decreases the affinity of the 20-mer for the total DNA-binding site of the helicase. Moreover, saturation of both the strong and weak nucleotide-binding sites of the enzyme with the ATP analogue further decreases the binding constant K_{20}, without significantly affecting the value of ΔF_{max} (see the Discussion).

Association of the ssDNA 10- and 20-mer, with the Proper and Total DNA-Binding Sites of the PriA Helicase with the ADP Bound to the Strong and ATPγS Bound to the Weak Nucleotide-Binding Sites of the Enzyme. Using independently obtained binding parameters characterizing the binding of ADP and ATPγS to the strong and weak nucleotide-binding sites of the PriA helicase (*46*), we can examine the effect of the mixed nucleotide state of the enzyme, i.e., with the strong nucleotide-binding site predominantly saturated with ADP and the weak site predominantly saturated with the ATP analogue, on the interactions of the helicase with the ssDNA. This can be achieved by selecting appropriate concentrations of both cofactors. Thus, in a solution containing 5 mM ATPγS and 1.5×10^{-4} M ADP, the strong binding site of the enzyme is ~90% saturated with ADP, while the weak site is ~70% saturated with ATPγS (*46*).

Fluorescence titration of the ssDNA 10-mer, dϵA(pϵA)$_9$, with the PriA helicase in buffer C (pH 7.0, 20 °C), containing 20 mM NaCl and 15 mM $MgCl_2$, in the presence of 5 mM ATPγS and 1.5×10^{-4} M ADP, is shown in Figure 6a. An analogous fluorescence titration of the ssDNA 20-mer, dϵA-(pϵA)$_{19}$, is shown in Figure 6b. For a comparison, titrations of corresponding ssDNA oligomers, in the same solution conditions but in the absence of the nucleotide cofactors, are also included. The solid lines in parts a and b of Figure 6 are nonlinear least-squares fits of the fluorescence titration curve, performed as described above, using the single-site binding isotherm defined by eq 7. The obtained binding and spectroscopic parameters are included in Table 1. The behavior of the mixed-cofactor system, where the strong nucleotide-binding site predominantly saturated with ADP

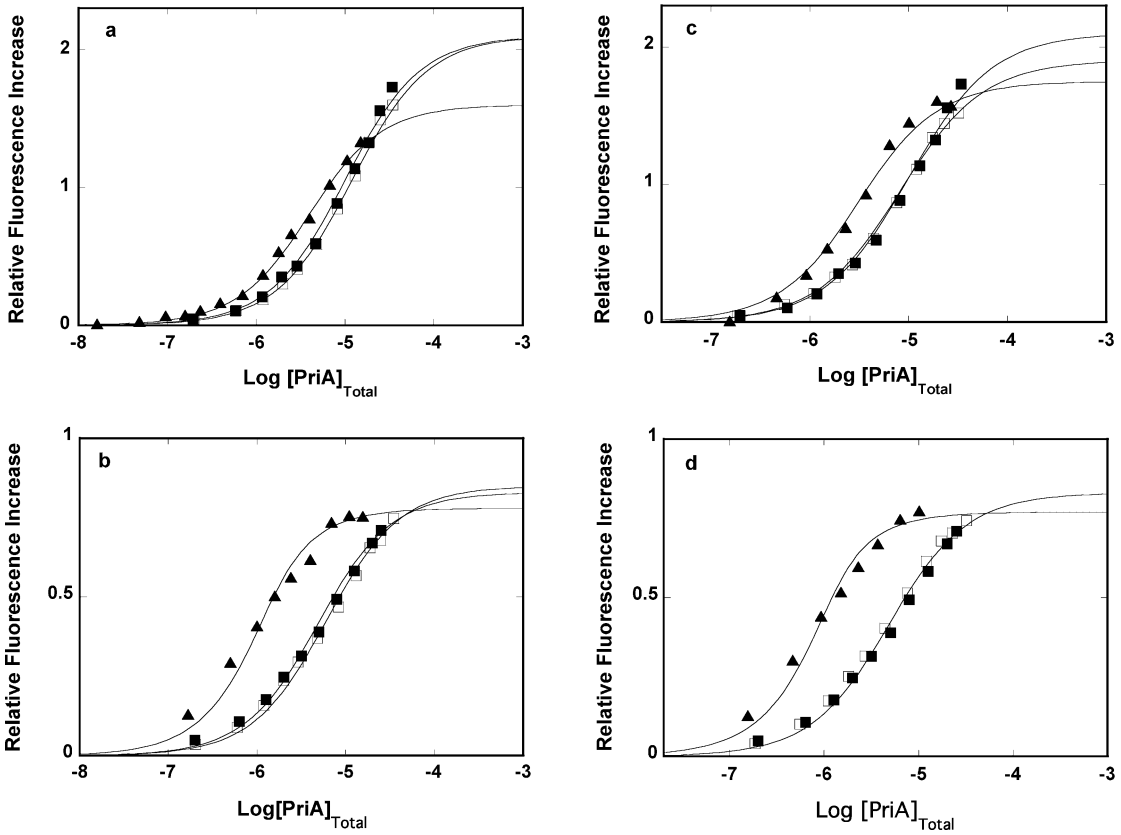

FIGURE 7: (a) Fluorescence titrations of the ssDNA 10-mer, dϵA(pϵA)$_9$, with the PriA helicase in buffer C (pH 7.0, 20 °C), containing 20 mM NaCl and 15 mM $MgCl_2$, in the absence and presence of different GDP concentrations: (■) 0 M, (□) 3×10^{-4} M, and (●) 10×10^{-3} M. The concentration of the ssDNA oligomer is 1×10^{-6} M. The solid lines are nonlinear least-squares fits of the titration curves, to the single-site binding isotherm (eq 7), using binding and spectroscopic parameters included in Table 1. (b) Fluorescence titrations of the ssDNA 20-mer, dϵA(pϵA)$_{19}$, with the PriA helicase in buffer C (pH 7.0, 20 °C), containing 20 mM NaCl and 15 mM $MgCl_2$, in the absence and presence of different ATPγS concentrations: (■) 0 M, (□) 3×10^{-4} M, and (●) 10×10^{-3} M. The concentration of the ssDNA oligomer is 1×10^{-6} M. The solid lines are nonlinear least-squares fits of the titration curves, to the single-site binding isotherm (eq 7), using binding and spectroscopic parameters included in Table 1. (c) Fluorescence titrations of the ssDNA 10-mer, dϵA(pϵA)$_9$, with the PriA helicase in buffer C (pH 7.0, 20 °C), containing 20 mM NaCl and 15 mM $MgCl_2$, in the absence and presence of different TDP concentrations: (■) 0 M, (□) 1×10^{-3} M, and (●) 10×10^{-3} M. The concentration of the ssDNA oligomer is 1×10^{-6} M. The solid lines are nonlinear least-squares fits of the titration curves, to the single-site binding isotherm (eq 7), using binding and spectroscopic parameters included in Table 1. (d) Fluorescence titrations of the ssDNA 20-mer, dϵA(pϵA)$_{19}$, with the PriA helicase in buffer C (pH 7.0, 20 °C), containing 20 mM NaCl and 15 mM $MgCl_2$, in the absence and presence of different TDP concentrations: (■) 0 M, (□) 1×10^{-3} M, and (●) 10×10^{-3} M. The concentration of the ssDNA oligomer is 1×10^{-6} M. The solid lines are nonlinear least-squares fits of the titration curves, to the single-site binding isotherm (eq 7), using binding and spectroscopic parameters included in Table 1.

and the weak site contains ATPγS, is different from the behavior observed in the presence of the ADP or ATPγS alone, bound in corresponding nucleotide-binding sites (Figures 4a and 5a). The values of the binding constants, K_{10} and K_{20}, are similar to the values of the same parameters observed in the presence of ADP exclusively in the strong nucleotide-binding site. On the other hand, the values of K_{10} and K_{20} are detectably higher than their values observed when the ATPγS is occupying the weak site of the enzyme (Table 1). Moreover, the observed relative maximum fluorescence increase, ΔF_{max}, is significantly lower for both the 10- and 20-mer as compared to the value of the same parameter obtained in the absence of the nucleotide cofactors or in the presence of ADP or ATPγS bound in the corresponding binding site (see the Discussion).

Base Specificity of the Nucleoside Diphosphate Binding to the Strong and Weak Nucleotide-Binding Sites of the PriA Helicase on the Association of the ssDNA 10- and 20-mer, with the Proper and Total DNA-Binding Sites of the Enzyme. Unlike the weak nucleotide-binding site, the strong binding site shows a dominant preference for the adenosine cofactors (*46*). Therefore, to address the effect of the type of base of the cofactor, bound in the strong and in both nucleotide-binding sites, on the PriA helicase interactions with the ssDNA, we examined ssDNA binding to the proper and total DNA-binding sites of the enzyme in the presence of different cofactors. Fluorescence titrations of the ssDNA 10-mer, dϵA-(pϵA)$_9$, with the PriA helicase in buffer C (pH 7.0, 20 °C), containing 20 mM NaCl, 15 mM $MgCl_2$, in the absence and presence of 3×10^{-4} M, and 10 mM GDP, are shown in Figure 7a. The higher concentrations of GDP used in these experiments are dictated by the lower affinities of this cofactor for the nucleotide-binding sites of the helicase, as compared to ADP (*46*). Corresponding fluorescence titrations of the ssDNA 20-mer, dϵA(pϵA)$_{19}$, are shown in Figure 7b. The solid lines in parts a and b of Figure 7 are nonlinear least-squares fits of the fluorescence titration curves, performed as described above, using the single-site binding isotherm (eq 7).

The affinity of the proper DNA-binding site of the enzyme for the ssDNA is slightly lower, with the binding constant K_{10} decreasing from $(1.1 \pm 0.2) \times 10^5$ M^{-1}, in the absence

of the GDP, to $(8.7 \pm 2.2) \times 10^4$ M^{-1}, with the strong nucleotide-binding site saturated with GDP. The observed maximum fluorescence increases, $\Delta F_{max} = 2.1 \pm 0.3$, and remains within the experimental accuracy, unaffected by the presence of the cofactor. This is similar to the effect of ADP bound in the strong nucleotide-binding site (Figure 4a). However, saturation of both the strong and weak nucleotide-binding sites with GDP increases the affinity only to $K_{10} = (2.9 \pm 0.5) \times 10^5$ M^{-1}, as compared to $K_{10} = (1.0 \pm 0.2) \times 10^6$ M^{-1}, observed for ADP (Table 1). Moreover, the value of $\Delta F_{max} = 1.6 \pm 0.1$ is lower than the value of the same parameter observed in the absence of GDP (2.1 ± 0.2) and in the case where both nucleotide-binding sites are saturated with ADP (Figure 4a). Thus, GDP exerts an effect of similar nature on the interactions with the ssDNA in the proper DNA-binding site as observed for ADP, although to a significantly lesser extent. The same is true for the effect of GDP on the interactions of the ssDNA with the total DNA-binding site of the enzyme (Figure 7b), with $K_{20} = (2.0 \pm 0.4) \times 10^6$ M^{-1}, while the same binding constant for ADP is $(3.0 \pm 0.5) \times 10^7$ M^{-1} (Figure 4b).

Fluorescence titrations of the ssDNA 10- and 20-mer, dϵA-(pϵA)$_9$ and dϵA(pϵA)$_{19}$, with the PriA helicase in the absence and presence of 1 and 10 mM TDP, are shown in parts c and d of Figure 7. The solid lines in parts c and d of Figure 7 are nonlinear least-squares fits of the fluorescence titration curves, performed as described above, using the single-site binding isotherm (eq 7). The presence of the pyrimidine cofactor has a stronger effect on the ssDNA affinity for the proper DNA-binding site than GDP, with $K_{10} = (3.8 \pm 0.9) \times 10^5$ M^{-1} (see above). However, the value of $\Delta F_{max} = 1.8 \pm 0.1$ is higher than observed in the presence of the purine cofactor. TDP also induces a higher affinity of the total DNA-binding site for the ssDNA than GDP, with $K_{20} = (3.3 \pm 0.8) \times 10^6$ M^{-1} (Figure 7d). Nevertheless, as observed for GDP, the effect of the pyrimidine cofactor, TDP, on the PriA interactions with the ssDNA, in the proper and total DNA-binding sites, is much less pronounced than the effect induced by ADP (see the Discussion).

Association of the ssDNA 10- and 20-mer with the Proper and Total DNA-Binding Sites of the PriA Helicase in the Presence of dADP Bound to the Strong and Weak Nucleotide-Binding Sites of the Enzyme. Because PriA helicase is a potent dATPase and dATP can support the dsDNA unwinding reaction catalyzed by the enzyme, we examine the effect of dADP on the ssDNA binding to the proper and total DNA-binding sites of the PriA helicase (*18*−*20*). Moreover, unlike any other nucleoside diphosphate, dADP binds to the strong and weak nucleotide-binding sites of the enzyme with an affinity and cooperativity very similar to ADP (*46*). Fluorescence titrations of the ssDNA 10-mer, dϵA(pϵA)$_9$, with the PriA helicase in buffer C (pH 7.0, 20 °C), containing 20 mM NaCl and 15 mM $MgCl_2$, in the absence and presence of 1×10^{-5} M and 10 mM dADP, are shown in Figure 8a. The corresponding titrations of the 20-mer, dϵA(pϵA)$_{19}$, are shown in Figure 8b. The solid lines in parts a and b of Figure 8 are nonlinear least-squares fits of the fluorescence titration curves, performed as described above, using the single-site binding isotherm (eq 7).

The effect of dADP on ssDNA binding to the proper DNA-binding site is significantly different from the behavior observed in the presence of ADP (Figure 4a). Similar to

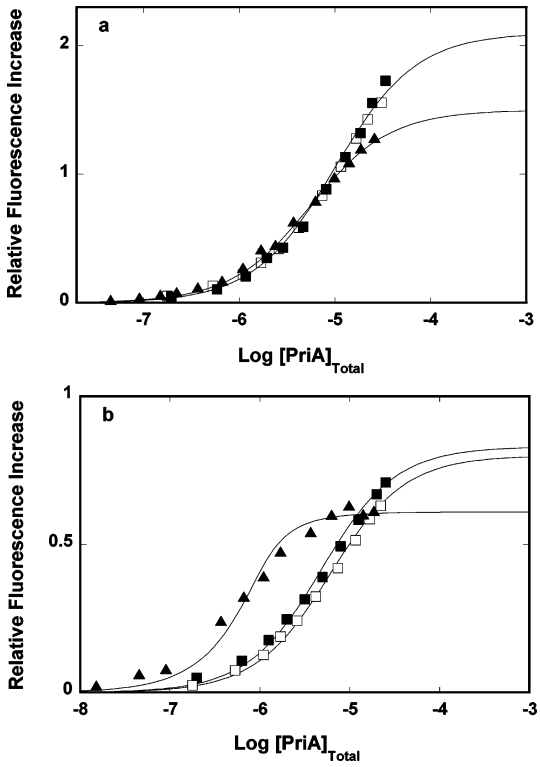

FIGURE 8: (a) Fluorescence titrations of the ssDNA 10-mer, dϵA-(pϵA)$_9$, with the PriA helicase in buffer C (pH 7.0, 20 °C), containing 20 mM NaCl and 15 mM $MgCl_2$, in the absence and presence of different dADP concentrations: (■) 0 M, (□) 1×10^{-5} M, and (●) 10×10^{-3} M. The concentration of the ssDNA oligomer is 1×10^{-6} M. The solid lines are nonlinear least-squares fits of the titration curves, to the single-site binding isotherm (eq 7), using binding and spectroscopic parameters included in Table 1. (b) Fluorescence titrations of the ssDNA 20-mer, dϵA(pϵA)$_{19}$, with the PriA helicase in buffer C (pH 7.0, 20 °C), containing 20 mM NaCl and 15 mM $MgCl_2$, in the absence and presence of different dADP concentrations: (■) 0 M, (□) 1×10^{-5} M, and (●) 10×10^{-3} M. The concentration of the ssDNA oligomer is 1×10^{-6} M. The solid lines are nonlinear least-squares fits of the titration curves, to the single-site binding isotherm (eq 7), using binding and spectroscopic parameters included in Table 1.

ADP, dADP bound to the strong site minimally affects the ssDNA binding to the proper DNA-binding site. However, saturation of both the strong and weak nucleotide-binding sites with dADP increases the binding constant from $K_{10} = (1.1 \pm 0.2) \times 10^5$ M^{-1} to only $K_{10} = (2.0 \pm 0.4) \times 10^5$ M^{-1}, as compared to $K_{10} = (1.0 \pm 0.2) \times 10^6$ M^{-1}, observed in the case of ADP (Table 1). This is even a lower increase of the affinity than obtained for GDP or TDP, saturating both nucleotide-binding sites (parts a and c of Figure 7). Moreover, the value of $\Delta F_{max} = 1.5 \pm 0.1$ is significantly lower than the value of the same parameter observed in the absence of the cofactor (2.1 ± 0.2) and where both nucleotide-binding sites are saturated with ADP ($\Delta F_{max} = 1.8 \pm 0.1$) (Figure 4a). In the case of the total DNA-binding site, dADP bound exclusively to the strong nucleotide-binding site slightly diminishes the ssDNA affinity with a minimal effect on the value of ΔF_{max}. This is similar to both ADP and the other nucleoside diphosphates (Figure 4a and parts b and d of Figure 7). However, unlike ADP, saturation of both nucleotide-binding sites with dADP increases the value of K_{20} to only $(6.0 \pm 1) \times 10^6$ M^{-1}, a factor of ~5 lower than the value observed for ADP (Figure 4b and Table 1). Moreover, instead of an increase of ΔF_{max}, as obtained for ADP (Figure

4b), a decrease of ΔF_{max} is observed, with $\Delta F_{max} = 0.61 \pm 0.05$ (Figure 8b). Thus, the effect of dADP resembles more the effect of GDP or TDP on the ssDNA interactions with the proper and total DNA-binding sites than that of ADP. This is despite the fact that dADP has the same base as ADP and binds with the affinity very close to the affinity of ADP, i.e., significantly higher than the affinities of GDP or TDP (*46*) (see the Discussion).

Kinetics of ssDNA Binding to the Proper DNA-Binding Site of the PriA Helicase in the Presence of ADP. The dynamics of the dramatic effect of saturating both nucleotide-binding sites of the PriA helicase with ADP on the enzyme interactions with the ssDNA has further been addressed using the fluorescence stopped-flow technique, by monitoring the fluorescence of the nucleic acid (*18*−*20*). In the first set of experiments, we examined the kinetics of the interactions of the proper DNA-binding site of the helicase with the ssDNA by examining the mechanism of binding ssDNA 10-mer, dϵA(pϵA)$_9$, to the enzyme (*18*−*20*).

The fluorescence stopped-flow kinetic traces of the ssDNA 10-mer, dϵA(pϵA)$_9$, after mixing dϵA(pϵA)$_9$ with a large excess of PriA helicase (pseudo-first-order conditions with respect to the DNA) in buffer C (pH 7.0, 10 °C), containing 20 mM NaCl and 15 mM $MgCl_2$, are described by a single-exponential function, at all examined concentrations of the protein (data not shown). This is different from the kinetics of the ssDNA binding in the absence or presence of a low magnesium concentration (2×10^{-4} M), examined by us previously, where two relaxation processes were observed (*20*). These data indicate that the elevated magnesium concentration eliminates one of the normal modes of the reaction (*20*). On the other hand, the observed amplitude accounts for the total amplitude of the overall relaxation process, as also previously observed, indicating that there is no loss of the signal in the instrument dead time (*20*, *47*). The dependence of the reciprocal relaxation time, $1/\tau_2$, upon the total concentration of PriA is shown in Figure 9a. The plot could, within experimental accuracy, suggest that a single bimolecular step is observed. However, Figure 9b shows the normalized amplitude of the observed relaxation step, as a function of the logarithm of the PriA concentration (*47*). It is evident that the amplitude experiences minimal, if any, dependence upon the protein concentration. Such behavior of the amplitude is incompatible with a single-step association, in examined conditions (*20*, *37*−*41*). Moreover, the value of the equilibrium binding constant, $K \sim 3.3 \times 10^7$ M^{-1}, obtained from the plot in Figure 9a, is ~2 order of magnitude larger than the value directly determined in the equilibrium titration, $K = (1.1 \pm 0.3) \times 10^5$ M^{-1}, clearly indicating that a more complex binding mechanism is occurring.

The simplest mechanism that can describe the observed dependence of the relaxation time and the amplitude upon the PriA concentration and the equilibrium thermodynamic data is a sequential reaction in which the PriA helicase binds the ssDNA in a very fast bimolecular step, followed by one first-order transition of the formed protein−ssDNA complex, as described by Scheme 1 (*20*, *37*−*41*). Because the rate of the bimolecular step is very fast, the relaxation time, characterizing the first normal mode of the reaction, is beyond the resolution of the stopped-flow technique. Therefore, at the elevated Mg^{2+} concentration, the mechanism of the ssDNA binding to the proper DNA-binding site of the PriA helicase is of the same sequential nature, as observed before, in the absence of Mg^{2+}, although one less intramolecular transition is observed (*20*).

The analysis of the relaxation data in parts a and b of Figure 9 is initiated by numerical nonlinear, least-squares fitting of the relaxation time (Figure 9a). Because of the fast rate, the bimolecular step equilibrates before the transition to the next intermediate takes place, allowing us to use the overall partial equilibrium constant, $K_1 = k_1/k_{-1}$, as a fitting parameter (Scheme 1). The analysis is facilitated by the fact that we also know the value of the overall macroscopic binding constant, $K_{10} = (1.1 \pm 0.3) \times 10^5$ M^{-1}, for the enzyme binding to the ssDNA 10-mer (Table 1). The macroscopic binding constant, K_{10}, is related to the bimolecular partial equilibrium constant, K_1, and the partial equilibrium constant, K_2, characterizing the intramolecular transition, by

$$K_{10} = K_1(1 + K_2) \tag{8}$$

where $K_2 = k_2/k_{-2}$ (Scheme 1). The above relationship reduces the number of independent parameters, in the relaxation time analysis, from three to two. Subsequently, the obtained rate constants are used as starting values in the fitting of the amplitude and extracting relative molar fluorescence parameters, F_1 and F_2, of $(P)_1$ and $(P)_2$ intermediates, respectively. This is accomplished using the matrix projection operator technique (*20*, *37*−*41*, *47*). This part of the analysis uses the value of the maximum relative increase of the ssDNA fluorescence accompanying the complex formation, $\Delta F_{max} = 2.1 \pm 0.3$, that is known from independent equilibrium fluorescence titrations (Table 1). The ΔF_{max} parameter can be analytically expressed as (*20*, *37*−*41*)

$$\Delta F_{max} = \frac{\Delta F_1 + K_2 \Delta F_2}{1 + K_2} \tag{9}$$

where $\Delta F_1 = (F_1 - F_o)/F_o$ and $\Delta F_2 = (F_2 - F_o)/F_o$ are fractional fluorescence intensities of each intermediate in the formation of the complex, relative to the molar fluorescence intensity of the free DNA oligomer, F_o (*20*, *37*−*41*, *47*). Equation 9 provides an additional relationship among the fitted parameters, thus, decreasing the number of independent variables and providing a scaling factor (*20*, *37*−*41*). The solid lines in parts a and b of Figure 9 are nonlinear least-squares fits of the relaxation time and amplitude, according to the mechanism defined by Scheme 1, using a single set of rates and spectroscopic parameters. The obtained rate constants and relative molar fluorescence intensities are included in Table 2.

A comparison between the value of the partial equilibrium constant, $K_1 = (2.1 \pm 0.7) \times 10^4$ M^{-1}, with the overall equilibrium constant $K_{10} = (1.1 \pm 0.3) \times 10^5$ M^{-1} indicates that the fast, bimolecular step provides the major part of the free energy of binding, $\Delta G°$, of the enzyme to the ssDNA. Nevertheless, a very low, if any, fluorescence change of the nucleic acid in this step strongly suggests the lack of any significant conformational changes of the nucleic acid structure accompanying the formation of the $(P)_1$ intermediate (Table 2) (*20*, *37*−*41*). The transition to the second inter-

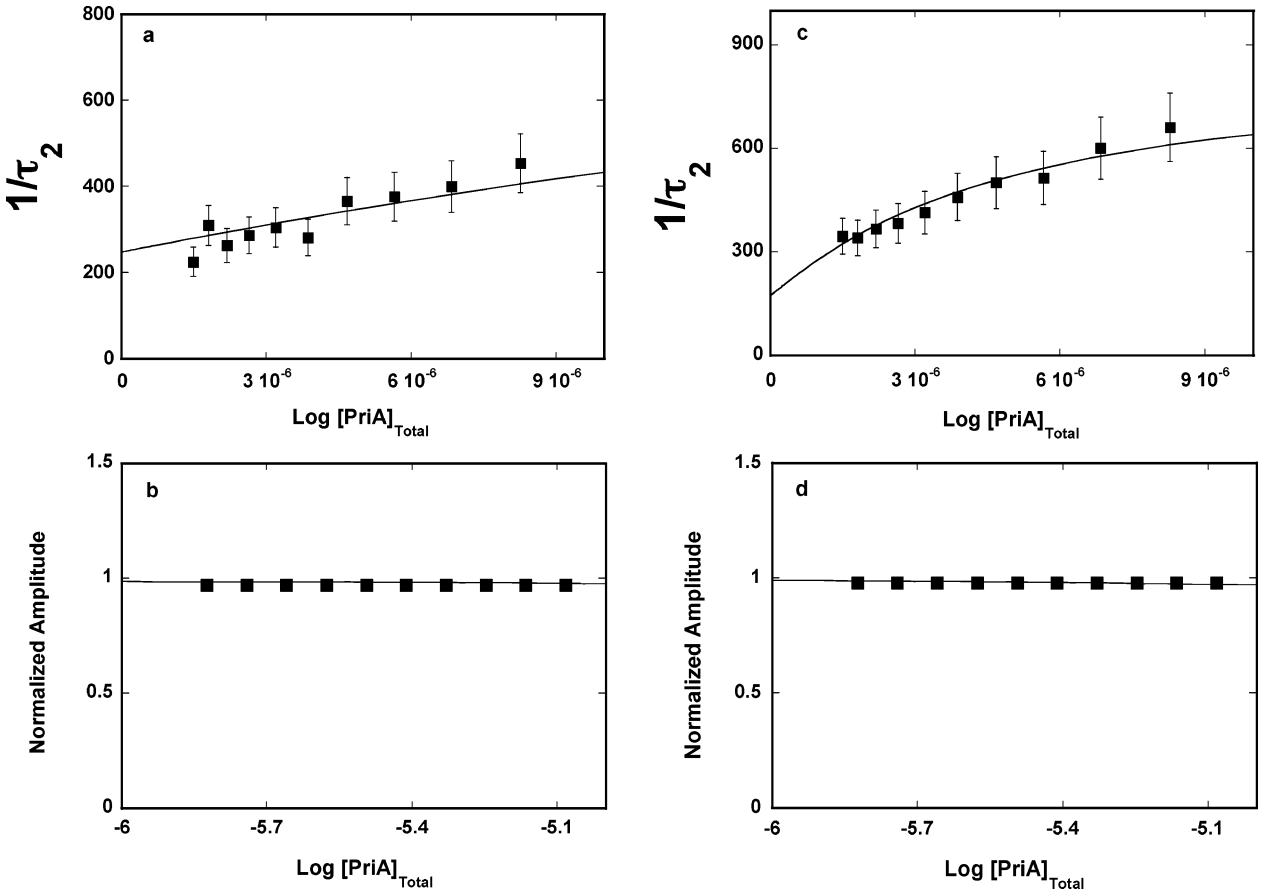

FIGURE 9: (a) Dependence of the reciprocal relaxation time, $1/\tau_2$, for the binding of the ssDNA 10-mer, dϵA(pϵA)$_9$, to the proper DNA-binding site of the PriA helicase in buffer C (pH 7.0, 20 °C), containing 20 mM NaCl and 15 mM $MgCl_2$, upon the total concentration of the enzyme. The solid line is the nonlinear least-squares fit according to the two-step sequential mechanism, defined by Scheme 1, with the equilibrium and rate constants: $K_1 = 2.08 \times 10^4$ M^{-1}, $k_2 = 1100$ s^{-1}, and $k_{-2} = 250$ s^{-1} (details in the text). The error bars are standard deviations obtained from three to four independent experiments. (b) Dependence of the normalized relaxation amplitude, for the binding of the ssDNA 10-mer, dϵA(pϵA)$_9$, to the proper DNA-binding site of the PriA helicase in buffer C (pH 7.0, 20 °C), containing 20 mM NaCl and 15 mM $MgCl_2$, upon the logarithm of the total enzyme concentration. The solid line is the nonlinear least-squares fit according to the two-step sequential mechanism, defined by Scheme 1, with the relative fluorescence intensities $F_1 = 1.18$ and $F_2 = 3.54$. The maximum nucleic acid fluorescence increase is taken from the equilibrium fluorescence titration in the same solution conditions as $\Delta F_{max} = 2.1$ (details in the text). The rate constants are the same as in a. (c) Dependence of the reciprocal relaxation time, $1/\tau_2$, for the binding of the ssDNA 10-mer, dϵA(pϵA)$_9$, to the proper DNA-binding site of the PriA helicase in buffer C (pH 7.0, 20 °C), containing 20 mM NaCl, 15 mM $MgCl_2$, and 5 mM ADP, upon the total concentration of the enzyme. The solid line is the nonlinear least-squares fit according to the two-step sequential mechanism, defined by Scheme 1, with the equilibrium and rate constants: $K_1 = 2.06 \times 10^5$ M^{-1}, $k_2 = 700$ s^{-1}, and $k_{-2} = 175$ s^{-1} (details in the text). The error bars are standard deviations obtained from three to four independent experiments. (d) Dependence of the normalized relaxation amplitudes, for the binding of the ssDNA 10-mer, dϵA(pϵA)$_9$, to the proper DNA-binding site of the PriA helicase in buffer C (pH 7.0, 20 °C), containing 20 mM NaCl, 15 mM $MgCl_2$, and 5 mM ADP, upon the logarithm of the total enzyme concentration. The solid line is the nonlinear least-squares fit according to the two-step sequential mechanism, defined by Scheme 1, with the relative fluorescence intensities $F_1 = 1.08$ and $F_2 = 3.24$. The maximum nucleic acid fluorescence increase is taken from the equilibrium fluorescence titration in the same solution conditions as $\Delta F_{max} = 1.8$ (details in the text). The rate constants are the same as in c. The nucleic acid concentration, 3×10^{-7} M, is the same in a−d.

Scheme 1

$$\mathrm{PriA + ssDNA} \underset{k_{-1}}{\overset{k_1}{\leftrightarrow}} (\mathrm{P})_1 \underset{k_{-2}}{\overset{k_2}{\leftrightarrow}} (\mathrm{P})_2$$

mediate, $(P)_2$, is also a fast process with the forward rate constant, $k_2 \approx 1100$ s^{-1} (Table 2). However, contrary to the $(P)_1$ intermediate, there is a large molar fluorescence increase ($F_2 = 3.5 \pm 0.2$) accompanying the formation of $(P)_2$, an indication of a large conformational change of the DNA, as compared to the free nucleic acid, in the complex (*20*−*24*, *37*−*41*). Nevertheless, the value of $k_{-2} \approx 250$ s^{-1} indicates that the enzyme can quickly return to the $(P)_1$ intermediate. The obtained rate constants for the second step provide the partial equilibrium constant $K_2 \approx 4.4$. Thus, the second step contributes favorably, although modestly, to the $\Delta G°$.

Analogous fluorescence stopped-flow kinetic traces of the ssDNA 10-mer, dϵA(pϵA)$_9$, after mixing dϵA(pϵA)$_9$ with a large excess of PriA helicase, in the presence of 5 mM ADP, are also described by a single-exponential function, at all examined concentrations of the protein, and the observed amplitude accounts for the total amplitude of the overall relaxation process (data not shown). At this ADP concentration, both nucleotide-binding sites of the helicase are engaged in interactions with the cofactor (*46*). The dependence of the reciprocal relaxation time, $1/\tau_2$, upon the total concentration of PriA is shown in Figure 9c. Similarly to the behavior observed in the absence of ADP, the plot would suggest a single bimolecular step. However, the normalized amplitude of the observed relaxation step, as a function of the logarithm of the PriA concentration, included in Figure 9d, shows a

Table 2: Kinetic, Thermodynamic, and Spectroscopic Papameters for PriA Helicase Binding to SsDNA Oligomers, dϵA(pϵA)$_9$ and dϵA(pϵA)$_{19}$, in Buffer C (pH 7.0, 20 °C), Containing 20 mM NaCl and 15 mM $MgCl_2$, in the Absence and Presence of ADP

10-mer, dϵA(pϵA)$_9$								
buffer	K_{10}[a] (M^{-1})	K_1 (M^{-1})	k_2 (s^{-1})	k_{-2} (s^{-1})	K_2	F_1[b]	F_2[b]	ΔF_{max}[a]
no ADP	$(1.1 \pm 0.4) \times 10^5$	$(2.1 \pm 0.7) \times 10^4$	1100 ± 140	250 ± 30	4.4 ± 1.2	1.18 ± 0.08	3.5 ± 0.2	2.1 ± 0.3
5 mM ADP	$(1.0 \pm 0.4) \times 10^6$	$(2.1 \pm 0.7) \times 10^5$	700 ± 80	175 ± 20	4.0 ± 1.2	1.08 ± 0.08	3.20 ± 0.2	1.8 ± 0.3
20-mer, dϵA(pϵA)$_{19}$								
buffer	K_{20}[a] (M^{-1})	K_1 (M^{-1})	k_2 (s^{-1})	k_{-2} (s^{-1})	K_2	F_1[b]	F_2[b]	ΔF_{max}[a]
no ADP	$(2.3 \pm 0.8) \times 10^5$	$(5.0 \pm 0.8) \times 10^4$	890 ± 100	225 ± 30	4.0 ± 1.2	1.02 ± 0.08	2.0 ± 0.1	0.83 ± 0.15
5 mM ADP	$(3.0 \pm 1.5) \times 10^7$	$(5.5 \pm 0.9) \times 10^5$	1080 ± 110	20 ± 3	54 ± 15	1.00 ± 0.08	1.9 ± 0.1	0.87 ± 0.15

[a] Determined in independent fluorescence titrations (details in the text). [b] Values are relative to the fluorescence, $F_1 = 1$, of the free dϵA(pϵA)$_N$ (details in the text).

minimal dependence upon the protein concentration, and the overall binding constant, $K_{10} \sim 5.3 \times 10^7$ M^{-1}, indicated by the plot, is significantly higher that $K_{10} = (1.0 \pm 0.3) \times 10^6$ M^{-1}, obtained from equilibrium titration (Table 1). These data are incompatible with the single-step association (*20*, *37*−*41*). Therefore, the simplest mechanism that can describe the observed dependence of the relaxation time and amplitude upon the PriA concentration in the presence of ADP, saturating both nucleotide-binding sites, is also the sequential two-step reaction described by Scheme 1. In other words, ADP does not change the mechanism of the ssDNA binding to the proper DNA-binding site of the PriA helicase, although it affects the energetics of the intermediates (see below).

The analysis of the relaxation data in parts c and d of Figure 9 has been performed in the same way as described for the data obtained in the absence of ADP. We utilize the fact that we know the value of the overall macroscopic binding constant, $K_{10} = (1.0 \pm 0.3) \times 10^6$ M^{-1}, for the enzyme binding to the ssDNA 10-mer in the presence of ADP, which is related to the bimolecular partial equilibrium constants, K_1 and K_2, by eq 8. Moreover, the value of the maximum relative increase of the ssDNA fluorescence, accompanying the complex formation, $\Delta F_{max} = 1.8 \pm 0.3$, is also known from independent equilibrium fluorescence titrations (Table 1) and related to the fractional fluorescence intensities of each intermediate, relative to the molar fluorescence intensity of the free DNA oligomer, by eq 9. The solid lines in parts c and d of Figure 9 are nonlinear least-squares fits of the relaxation time and amplitude, according to the mechanism defined by Scheme 1, using a single set of rate and spectroscopic parameters, included in Table 2.

The obtained data indicate that the major effect of ADP, bound to both nucleotide-binding sites of the enzyme, on the ssDNA binding to the proper DNA-binding site is expressed in the value of the partial equilibrium constant, $K_1 = (2.1 \pm 0.7) \times 10^5$ M^{-1}, which is an order of magnitude larger than $K_1 = (2.1 \pm 0.7) \times 10^4$ M^{-1}, observed in the absence of ADP (Table 2). However, the lack of a fluorescence change of the nucleic acid in this step strongly suggests the lack of conformational changes of the nucleic acid, accompanying the formation of the $(P)_1$ intermediate, similar to the behavior observed in the absence of ADP (*20*, *37*−*41*). On the other hand, both dynamics and energetics of the transition to the second intermediate, $(P)_2$, is not affected by ADP, with the partial equilibrium constant $K_2 \approx 4.0$, as compared to $K_2 \approx 4.4$, observed in the absence of ADP. Nevertheless, there is a large molar fluorescence increase ($F_2 = 3.2 \pm 0.2$) accompanying the formation of $(P)_2$, indicating a large conformational change of the DNA, as compared to the free nucleic acid (*20*−*24*, *37*−*41*).

Kinetics of ssDNA Binding to the Total DNA-Binding Site of the PriA Helicase in the Presence of ADP. The fluorescence stopped-flow studies of the ssDNA 20-mer, dϵA-(pϵA)$_{19}$, binding to the total DNA-binding site of the PriA helicase have been performed in an analogous way as described for the ssDNA 10-mer. In the absence of ADP, the time courses are described by a single-exponential function, at all examined concentrations of the protein (data not shown). The dependence of the reciprocal relaxation time, $1/\tau_2$, upon the total concentration of PriA is shown in Figure 10a. The plot of the normalized amplitude of the observed relaxation step, as a function of the logarithm of the PriA concentration is shown in Figure 10b. Both, the absence of a dependence of the amplitude upon [PriA] and the value of the equilibrium binding constant, $K \sim 3.3 \times 10^7$ M^{-1}, obtained from the plot in Figure 10a, ~2 orders of magnitude larger than the value directly determined in equilibrium titration, $K = (2.3 \pm 0.8) \times 10^5$ M^{-1}, indicate that the simplest mechanism that can describe the observed dependence of the relaxation time and amplitude upon the PriA concentration and the equilibrium thermodynamic data is a sequential reaction, described by Scheme 1. Analysis of the kinetic data has been performed as described above. The solid lines in parts a and b of Figure 10 are nonlinear least-squares fits of the relaxation time and amplitude, according to the mechanism defined by Scheme 1, using a single set of rate and spectroscopic parameters. The obtained rate constants and relative molar fluorescence intensities are included in Table 2. It is clear that, in the absence of ADP, the rate and thermodynamic parameters for the binding of the 20-mer to the total DNA-binding site are very similar to the same parameters obtained for the 10-mer binding, exclusively, to the proper DNA-binding site of the helicase (see the Discussion) (*18*−*20*).

The situation is different in the presence of 5 mM ADP, where both nucleotide-binding sites of the helicase are engaged in interactions with the cofactor (*46*). Although the mechanism remains the same and described by Scheme 1, the energetics and dynamics of the reaction intermediates are dramatically affected by the presence of ADP. The dependence of the reciprocal relaxation time, $1/\tau_2$, upon the total concentration of PriA is shown in Figure 10c, and the normalized amplitude, as a function of the logarithm of the PriA concentration, is included in Figure 10d. The analysis of the relaxation data in parts c and d of Figure 10 has been

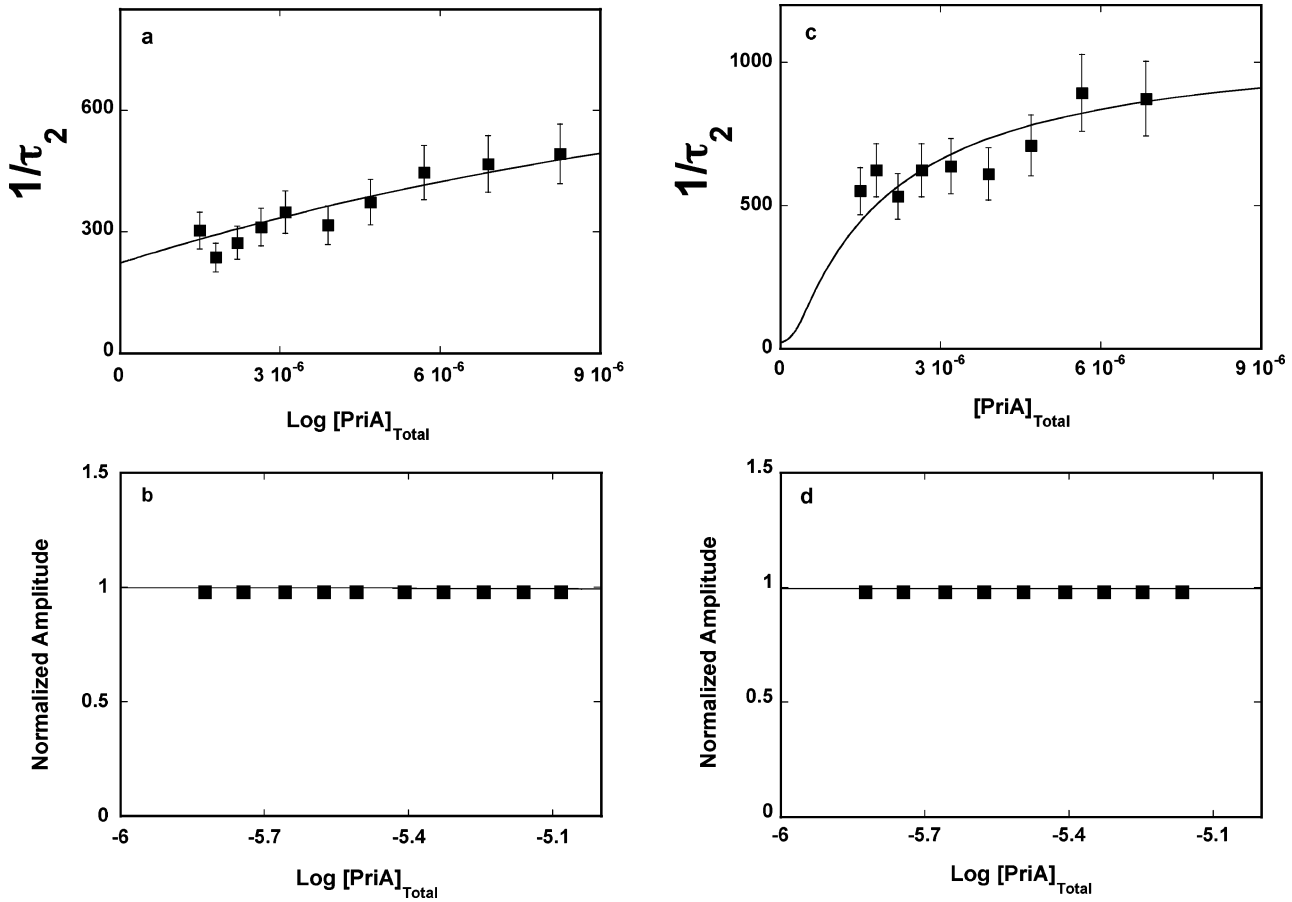

FIGURE 10: (a) Dependence of the reciprocal relaxation time, $1/\tau_2$, for the binding of the ssDNA 20-mer, dϵA(pϵA)$_{19}$, to the total DNA-binding site of the PriA helicase in buffer C (pH 7.0, 20 °C), containing 20 mM NaCl and 15 mM $MgCl_2$, upon the total concentration of the enzyme. The solid line is the nonlinear least-squares fit according to the two-step sequential mechanism, defined by Scheme 1, with the equilibrium and rate constants: $K_1 = 5.0 \times 10^4$ M^{-1}, $k_2 = 890$ s^{-1}, and $k_{-2} = 225$ s^{-1} (details in the text). The error bars are standard deviations obtained from three to four independent experiments. (b) Dependence of the normalized relaxation amplitudes, for the binding of the ssDNA 20-mer, dϵA(pϵA)$_{19}$, to the total DNA-binding site of the PriA helicase in buffer C (pH 7.0, 20 °C), containing 20 mM NaCl and 15 mM $MgCl_2$, upon the logarithm of the total enzyme concentration. The solid line is the nonlinear least-squares fit according to the two-step sequential mechanism, defined by Scheme 1, with the relative fluorescence intensities $F_1 = 1.02$ and $F_2 = 2.04$. The maximum nucleic acid fluorescence increase is taken from the equilibrium fluorescence titration in the same solution conditions as $\Delta F_{max} = 0.83$ (details in the text). The rate constants are the same as in a. (c) Dependence of the reciprocal relaxation time, $1/\tau_2$, for the binding of the ssDNA 20-mer, dϵA(pϵA)$_{19}$, to the total DNA-binding site of the PriA helicase in buffer C (pH 7.0, 20 °C), containing 20 mM NaCl, 15 mM $MgCl_2$, and 5 mM ADP, upon the total concentration of the enzyme. The solid line is the nonlinear least-squares fit according to the two-step sequential mechanism, defined by Scheme 1, with the equilibrium and rate constants: $K_1 = 5.45 \times 10^5$ M^{-1}, $k_2 = 1080$ s^{-1}, and $k_{-2} = 20$ s^{-1} (details in the text). The error bars are standard deviations obtained from three to four independent experiments. (d) Dependence of the normalized relaxation amplitude, for the binding of the ssDNA 20-mer, dϵA(pϵA)$_{19}$, to the total DNA-binding site of the PriA helicase in buffer C (pH 7.0, 20 °C), containing 20 mM NaCl, 15 mM $MgCl_2$, and 5 mM ADP, upon the logarithm of the total enzyme concentration. The solid line is the nonlinear least-squares fit according to the two-step sequential mechanism, defined by Scheme 1, with the relative fluorescence intensities $F_1 = 0.99$ and $F_2 = 1.89$. The maximum nucleic acid fluorescence increase is taken from the equilibrium fluorescence titration in the same solution conditions as $\Delta F_{max} = 0.87$ (details in the text). The equilibrium and rate constants are the same as in c. The nucleic acid concentration, 3×10^{-7} M, is the same in a−d.

performed in the same way as described above. The solid lines in parts c and d of Figure 10 are nonlinear least-squares fits of the relaxation time and amplitude, according to the mechanism defined by Scheme 1, using a single set of rate and spectroscopic parameters, included in Table 2.

The obtained data indicate that, unlike in the case of the ssDNA 10-mer, which exclusively binds to the proper DNA-binding site of the helicase, the effect of ADP, bound to both nucleotide-binding sites of the enzyme, on the ssDNA binding, which can encompass the total DNA-binding site, is expressed in the values of both partial equilibrium constants, K_1 and K_2. The value of $K_1 = (5.5 \pm 0.9) \times 10^5$ M^{-1} is an order of magnitude larger than $K_1 = (5.0 \pm 0.8) \times 10^4$ M^{-1}, observed in the absence of ADP (Table 2). The forward rate constant of the transition to the second intermediate, $(P)_2$, $k_2 = 1080$ s^{-1}, is moderately increased, as compared to the same parameter, $k_2 = 890$ s^{-1}, obtained in the absence of the cofactor. However, the value of the backward rate constant, k_{-2}, is decreased by more than an order of magnitude, from ~225 to ~20 s^{-1} (Table 2). As a result, the partial equilibrium constant, K_2, is increased from ~4 to ~54, in the presence of ADP, and in turn, the second step has a strong and favorable contribution to the overall free energy of binding (see the Discussion).

DISCUSSION

Direct Communication Between Both Nucleotide-Binding Sites of the PriA Helicase and the DNA-Binding Site of the Enzyme. Strong quenching of the PriA protein emission upon binding of the TNP analogues of nucleotide cofactors to both

nucleotide-binding sites of the enzyme allows us to access the effect of the nucleic acid on the binding affinities and also on the structure of the nucleotide-binding sites, as sensed by the protein fluorescence. The ssDNA 10-mer binds exclusively to the proper DNA-binding site of the PriA helicase (*18*−*20*). Nevertheless, the ssDNA 10-mer exerts a very strong effect on the binding of the ADP analogue to both the strong and weak nucleotide-binding sites of the helicase (Figure 1). The affinities of both sites decrease by a similar factor of ∼20. Such a profound effect on affinities of both nucleotide-binding sites provides, independently of any binding models, strong evidence of direct and extensive communications between the nucleotide-binding sites and the proper DNA-binding site of the helicase.

However, the ssDNA, exclusively bound to the proper DNA-binding site, has a different effect on the structures of both binding sites. The relative quenching of the protein fluorescence accompanying the TNP-ADP binding to the strong site increases by ∼90% from $\Delta F_{1_{max}} = 0.2 \pm 0.03$ to 0.38 ± 0.03, while the analogous parameter for the weak site decreases by ∼50%, from $\Delta F_{2_{max}} = 0.64 \pm 0.08$ to 0.42 ± 0.08. As a result, in the presence of the 10-mer, the relative fluorescence quenching parameters, $\Delta F_{1_{max}}$ and $\Delta F_{2_{max}}$, have similar values, while in the absence of the nucleic acid, they differ by a factor of ∼3. Noticeably, the primary structure of the PriA helicase contains 15 tryptophan residues spread over the entire amino acid sequence of the protein (*11*, *12*). The values of both $\Delta F_{1_{max}}$ and $\Delta F_{2_{max}}$ indicate that a large number of tryptophan residues are affected by the binding of the ADP analogue in the presence of the ssDNA 10-mer, indicating that the communication between both nucleotide-binding sites and the proper DNA-binding site includes conformational changes that involve the entire protein molecule.

The effect of the ssDNA 20-mer, which encompasses the total DNA-binding site of the helicase, on the TNP-ADP affinities for the strong and weak nucleotide-binding sites is similar, although not identical, to the effect exerted by the 10-mer. This similarity indicates that major conformational changes of the protein in the complex with the nucleic acid that affect both nucleotide-binding sites are already induced by the nucleic acid associated with the proper DNA-binding site. Nevertheless, in the presence of the 20-mer, the value of $\Delta F_{1_{max}}$ 0.28 ± 0.03; i.e., it is increased to a lesser extent, as observed for the 10-mer ($\Delta F_{1_{max}} = 0.38 \pm 0.03$). On the other hand, the value of $\Delta F_{2_{max}} = 0.37 \pm 0.03$ is lower than the value of the corresponding parameter in the presence of the 10-mer ($\Delta F_{2_{max}} = 0.42 \pm 0.08$). In other words, the 20-mer induces conformational changes in the protein molecule of a similar nature as the 10-mer but of a detectable different magnitude. This behavior of the relative quenching parameters of the protein fluorescence provides the first indication that the 20-mer engages in additional interactions and/or a different area of the total DNA-binding site, beyond the proper DNA-binding site (see below).

DNA Induces Dramatic Changes in the Structure of the Weak Nucleotide-Binding Site, as Compared to Only Moderate Structural Changes of the Strong Nucleotide-Binding Site Induced by the Nucleic Acid. The changes of the tryptophan emission quenching, accompanying the binding of the TNP-nucleotide analogues to the PriA helicase in the presence of the ssDNA, provide direct evidence of the conformational changes of the entire protein molecule, induced by the nucleic acid binding (see above). However, as such, they do not indicate the nature of the structural changes occurring in the nucleotide-binding sites. Fluorescence of the TNP analogues offers a means to directly access the structure of the nucleotide-binding sites. In a companion paper (*47*), we have determined the relative fluorescence increases accompanying the binding of the TNP analogues to the strong and weak nucleotide-binding sites of the PriA helicase, in the absence of the nucleic acid. Both binding sites differ strongly in the extent of the induced fluorescence increase, and this difference is particularly pronounced in the absence of magnesium. In the case of the ADP analogue, $\Delta F_{1_{max}} = 12.0 \pm 0.3$ and $\Delta F_{2_{max}} = 0.3 \pm 0.1$. Thus, the cofactor is placed in an environment of a low polarity in the strong site, but the environment of the weak site is barely different from the bulk solvent (*30*−*33*, *47*). On the other hand, in the presence of the ssDNA 10-mer, the same fluorescence parameters are $\Delta F_{1_{max}} = 8.0 \pm 0.3$ and $\Delta F_{2_{max}} = 8.0 \pm 2.0$, respectively. It is evident that the bound nucleic acid very differently affects the structure of the strong and weak nucleotide-binding sites. The polarity of the strong site is diminished, as indicated by the ∼30% lower value of $\Delta F_{1_{max}}$, while the polarity of the weak site dramatically increases, with the value of $\Delta F_{2_{max}}$ larger by a factor of ∼27. As a result, in the presence of the nucleic acid, the value of $\Delta F_{2_{max}}$ becomes the same as the value of $\Delta F_{1_{max}}$, observed for the strong site; i.e., in the presence of the nucleic acid, TNP-ADP experiences, in both nucleotide-binding sites, an environment of the same polarity.

In the absence of the DNA and magnesium, the relative fluorescence increases accompanying the binding of TNP-ATP to the strong and weak nucleotide-binding sites are $\Delta F_{1_{max}} = 12.4 \pm 0.3$ and $\Delta F_{2_{max}} = 0.3 \pm 1$ (*47*). In the presence of DNA, the same parameters are $\Delta F_{1_{max}} = 6.3 \pm 0.3$ and $\Delta F_{2_{max}} = 10.0 \pm 3.0$ (Figure 3b). Thus, the ATP analogue senses the changes of the nucleotide-binding sites induced by the nucleic acid of a similar nature as observed for the ADP analogue. However, the value of $\Delta F_{1_{max}}$ is diminished even more than in the case of TNP-ADP, while the value of $\Delta F_{2_{max}}$ is increased by a factor of ∼33, i.e., larger than the factor of ∼27 observed for the ADP analogue. Moreover, in the case of TNP-ATP, the value of $\Delta F_{2_{max}} = 10.0 \pm 3.0$ is now larger than the value of $\Delta F_{1_{max}} = 6.3 \pm 0.3$, indicating that TNP-ATP experiences an environment of lower polarity in the weak site than in the strong site. There are several important aspects of these findings. First, they provide additional and independent evidence of the communication between both nucleotide-binding sites and the proper DNA-binding site of the helicase (see above). Second, these data indicate that the observed changes in the structures of both nucleotide-binding sites are an intrinsic property of the PriA helicase, i.e., the response of the structure of the nucleotide-binding sites of the enzyme to the binding of the nucleic acid, independent of the number of phosphate groups of the bound nucleotide cofactor. Nevertheless, the differences between the ADP and ATP analogues strongly suggest that the cofactors are bound in different orientations in both nucleotide-binding sites. Finally, the particularly dramatic effect of the DNA on the structure of the weak nucleotide-binding site strongly indicates that the weak site is intimately involved in regulating the helicase interactions with the nucleic acid (see below).

The Strong Nucleotide-Binding Site of the PriA Helicase Does Not Directly Affect the Affinity of the Helicase for the ssDNA. The control of the affinity of an enzyme for its substrates by the ATP/ADP binding and/or hydrolysis is a common feature of the enzymes performing free-energy transduction (*42*, *43*). Thermodynamic and kinetic studies described in refs *46* and *47*, as well as available biochemical data, indicate that the strong nucleotide-binding site is the high-affinity ATPase site of the PriA helicase (*44*, *45*). Therefore, it seems surprising that neither ATPγS nor ADP binding to the strong nucleotide-binding site drastically affects the affinity of the PriA helicase for the ssDNA. In the presence of ADP, the affinity of the DNA is unaffected, while binding of ATPγS to the strong site even diminishes the enzyme affinity for the DNA. This is true for both the proper and total DNA-binding sites of the PriA helicase (parts a and b of Figure 4 and parts a and b of Figure 5). Nevertheless, the structure of the bound DNA is affected as indicated by the lower values of the relative fluorescence increases, observed for the helicase with the strong nucleotide-binding site saturated with ADP or ATPγS. These results indicate that the strong nucleotide-binding site does not directly control the affinity of the PriA helicase for the DNA, through the ATP or ADP binding, although it affects the structures of the bound DNA. Moreover, the fact that the bound DNA affects dramatically only the structure of the weak nucleotide-binding site indicates that the control of the enzyme affinity for the nucleic acid must involve both nucleotide-binding sites of the helicase (see below).

PriA Helicase with Both Nucleotide-Binding Sites Saturated with ADP but Not with ATP Analogue Has an Increased Affinity for the ssDNA Bound in the Proper and Total DNA-Binding Sites of the Enzyme. Unlike the exclusive binding of ADP to the strong nucleotide-binding site of the PriA helicase, binding of ADP to both nucleotide-binding sites of the enzyme increases its affinity for the ssDNA, bound in the proper DNA-binding site, by an order of magnitude (Figure 4a). Although such an increase of the affinity could result solely from the increase of the cooperative interactions between the bound ADP molecules, experiments with different nucleotide cofactors strongly suggest that this is not the case. In the presence of GDP or TDP, the increase of the affinity is also observed (parts a and c of Figure 7). However, the increase of the affinity is significantly lower than observed for ADP, although binding of GDP and TDP is characterized by cooperative interactions that are very similar to the cooperative interactions observed in the binding of ADP (*46*). In other words, the observed increase of the ssDNA affinity does not exclude the effect of cooperative interactions between the nucleotide-binding sites, but it must include a direct communication between the weak nucleotide-binding site and the proper DNA-binding site of the helicase (see above). The fact that ADP bound to the weak site induces an order of magnitude increase of the partial equilibrium constant, K_1, for the binding of the ssDNA to the proper DNA-binding site strongly supports this conclusion (Table 2).

On the other hand, saturation of both nucleotide-binding sites with ATPγS does not lead to an increased affinity of the enzyme for the nucleic acid. Contrary, the affinity is diminished (Figure 5a). Experiments with the mixture of ADP and ATPγS provide additional insight about the observed effects. When the strong site is saturated with ADP and the weak site is occupied by ATPγS, the enzyme affinity for the ssDNA is diminished. Notwithstanding, the observed relative fluorescence increase, ΔF_{max}, is significantly lower than observed in the presence of ADP, exclusively bound in the strong binding site, or ATPγS, bound in both the strong and weak sites. As we discussed before, the fluorescence of the etheno derivative of the DNA is predominantly affected by the structure of the nucleic acid and not the polarity of the environment (*21*−*24*, *35*). Thus, such a lower value of ΔF_{max} indicates a different nucleic acid structure in the presence of both cofactors, as compared to the structure observed in the presence of ADP or ATPγS alone (Figures 4a and 5a) (*21*−*24*, *35*, *36*). If ADP in the strong site was dominating the interactions with the DNA, one would observe an intact affinity and a much larger ΔF_{max}. If ATPγS in the weak nucleotide-binding site was dominating the DNA-binding process, one would observe even more diminished affinity and a much larger ΔF_{max}.

First, these data clearly show that the effect of the two nucleotide-binding sites on the DNA binding to the PriA helicase is not a simple sum of the effects originated from each site but depends upon the type of the nucleotide cofactor bound to each site. Second, the nature of the phosphate group of the cofactor in the weak binding site plays a major role in determining the affinity of the enzyme for the nucleic acid. However, it cannot induce the same affinity and structure of the nucleic acid, as observed when both sites are saturated, with the cofactor having the same phosphate group, if the strong binding site is associated with a different nucleotide. Thus, ATPγS, bound in the weak site, cannot induce lower ssDNA affinity, when ADP occupies the strong site, to the extent that is observed when the strong site is saturated with ATPγS. By the same token, ADP bound to the weak nucleotide-binding site will induce a significantly higher affinity of the helicase for the ssDNA and a suitable DNA structure only if another ADP molecule occupies the strong nucleotide-binding site. The high-affinity state of the PriA helicase for the ssDNA is the state where both nucleotide-binding sites of the enzyme are saturated with ADP.

Similar to ADP, binding of GDP or TDP to the strong nucleotide-binding site does not affect the PriA helicase affinity for the ssDNA (Figure 7). On the other hand, although GDP and TDP, bound to both nucleotide-binding sites of the PriA helicase, can induce a higher DNA affinity of the helicase than observed in the absence of cofactors, the effect is very modest as compared to the effect induced by ADP (Figure 7). Because the base specificity predominantly resides in the strong binding site, these results reinforce the conclusion of a very intricate interrelationship between both nucleotide-binding sites in controlling the enzyme affinity for the nucleic acid (see above). Interestingly, although dADP has the same base as ADP and it binds to both nucleotide-binding sites with the affinity and cooperativity similar to ADP, nevertheless, it does not induce the same increase of the DNA affinity as ADP (parts a and b of Figure 8). In effect, the magnitude of the dADP effect is more similar to the effects on the DNA affinity induced by GDP or TDP, particularly, for the proper DNA-binding site. Moreover, the structure of the DNA is different in the presence of the dADP, as indicated by significantly lower relative fluorescence increases of dϵA(pϵA)$_9$ and dϵA(pϵA)$_{19}$

in the complex with the helicase, as compared to the same parameters observed for ADP. These data strongly suggest that the orientation of the ssDNA in the complex with the helicase having both nucleotide-binding sites saturated with dADP is different than in the presence of ADP. This corroborates well with the current biochemical data that show less efficient hydrolysis of dATP than ATP by the enzyme in the presence of ssDNA (*39*). Altogether, these data point out two levels of communication within the PriA molecule, involving the type of the base, structure of the phosphate group, and the ribose of the bound cofactors. They include the communication among the nucleotide-binding sites as well as the communication between the sites and the DNA-binding site in inducing the high-affinity state of the helicase for the nucleic acid.

A Strong Increase of the Affinity of the PriA Helicase, with Both Nucleotide-Binding Sites Saturated with ADP, for the ssDNA 20-mer that Encompasses the Entire Total DNA-Binding Site of the Enzyme, Indicates that an Additional Area of the Protein Is Engaged in Interactions with the Nucleic Acid. As observed for the ssDNA 10-mer, the presence of ADP exclusively in the strong nucleotide-binding site has a minimal effect on the binding of the ssDNA 20-mer that encompasses the entire total DNA-binding site of the PriA helicase (Figure 4b). These data reinforce the conclusion that the strong nucleotide-binding site does not directly affect the helicase interactions with the ssDNA both in the proper and total DNA-binding sites (see above). However, saturation of both nucleotide-binding sites with ADP induces an even more pronounced effect on the PriA affinity for the ssDNA 20-mer than the effect observed for the ssDNA 10-mer exclusively bound in the proper DNA-binding site. The binding constant, K_{20}, is larger by an order of magnitude than K_{10}. As a result, the value of K_{20} is increased by more than 2 orders of magnitude as compared to the value of the same parameter in the absence of the cofactor or with ADP exclusively bound in the strong nucleotide-binding site (Figure 4b). Moreover, unlike the effect of ADP on the ΔF_{max} of the ssDNA 10-mer, bound exclusively in the proper DNA-binding site, the value of ΔF_{max} observed for the 20-mer is increased, indicating a different conformation of the bound nucleic acid (*18*, *19*, *21*−*24*, *35*, *36*).

Noticeably, such a dramatic increase of the ssDNA 20-mer affinity in the presence of ADP and an accompanying different conformational change of the 20-mer, dϵA(pϵA)$_{19}$, as compared to the 10-mer, dϵA(pϵA)$_9$, exclusively bound in the proper DNA-binding site, occurred only because of the increased length of the ssDNA that can now encompass the total DNA-binding site. The simplest explanation of such a behavior is that in the complex of the PriA helicase, with both nucleotide-binding sites of the enzyme saturated with ADP, an additional interacting area of the total DNA-binding site of the protein becomes engaged in interactions with the nucleic acid. The fact that the enzyme, saturated with ADP, binds only one 10-mer molecule indicates that this additional area has a significantly lower affinity for the DNA than the proper DNA-binding site and can only engage the DNA that is already bound in the proper site, i.e., when the local concentration of the nucleic acid is high. Otherwise, the PriA helicase would bind two ssDNA 10-mer molecules in the presence of ADP in the examined solution conditions, which is not experimentally observed (*18*−*20*). Moreover, thermodynamic and kinetic studies clearly showed that the overall as well as the partial binding constants of the PriA helicase for the ssDNA oligomers, in the absence of ADP, contain a statistical factor that can completely be accounted for by considering only the interactions of the DNA with the proper DNA-binding site (*18*−*20*). Therefore, these data also strongly suggest that the additional interacting area is not available to the ssDNA in the absence of ADP associated with both nucleotide-binding sites of the helicase.

A strong indication that an additional area of the total DNA-binding site becomes involved in interactions with the ssDNA comes from the kinetic studies described in this paper (Figures 9 and 10). In the absence of ADP or when the cofactor saturates only the strong nucleotide-binding site, both, the ssDNA 10- and 20-mer, bind with the same mechanism and very similar energetics and dynamics between the intermediates (Table 2). This is in excellent agreement with the conclusion from thermodynamic and kinetic studies that, in these conditions, only the proper DNA-binding site is engaging in interactions with the nucleic acid (*18*−*20*). When nucleotide-binding sites are both saturated with ADP, the partial equilibrium constant, K_1, increases by an order of magnitude for both the 10- and 20-mer, as a result of a direct communication between the weak nucleotide-binding site and the proper DNA-binding site (see above). However, while the partial equilibrium constant, K_2, for the 10-mer remains completely unaffected by the cofactor, the same parameter increases by more than an order of magnitude for the 20-mer. The 20-mer, which encompasses the total DNA-binding site, becomes additionally anchored in the DNA-binding site, resulting in a strong additional free-energy contribution to the overall binding process (Table 2). The anchoring process occurs after the first binding step, initiated through the proper DNA-binding site and experienced by both the 10- and 20-mer. Nevertheless, only the 20-mer is long enough to reach the additional interacting area of the total DNA-binding site.

The fact that the same transition of the protein−ssDNA complex, $(P)_1 \leftrightarrow (P)_2$, occurs for both the 10- and 20-mer and in the absence and presence of ADP, indicates that the $(P)_1 \leftrightarrow (P)_2$ transition is independent of the length of the DNA and the presence of the cofactor. In other words, the transition is an intrinsic property of the PriA helicase. The energetics and dynamics of both the 10- and 20-mer are similarly affected by the $(P)_1 \leftrightarrow (P)_2$ transition in the absence of the cofactor or with ADP bound only to the strong nucleotide-binding site. Noticeably, the transition occurs in the absence of ADP, yet the 20-mer cannot efficiently engage in additional interactions with the protein. This indicates that ADP binding to both nucleotide-binding sites specifically opens an additional area of interactions in the formed $(P)_2$ intermediate. The forward rate constant, k_2, for the 20-mer increases by only ~20%, as the $(P)_2$ intermediate is already formed, while the backward rate constant, k_{-2}, decreases by a factor of ~11, as additional interactions stabilize the complex. The ssDNA 10-mer, bound at the proper DNA-binding site cannot reach the additional interacting area. Consequently, the $(P)_1 \leftrightarrow (P)_2$ transition, with the 10-mer bound, is minimally affected by the presence of ADP.

A schematic model of the ADP effect on the PriA helicase interactions with the ssDNA that summarizes the data obtained in this paper is shown in Figure 11. As indicated

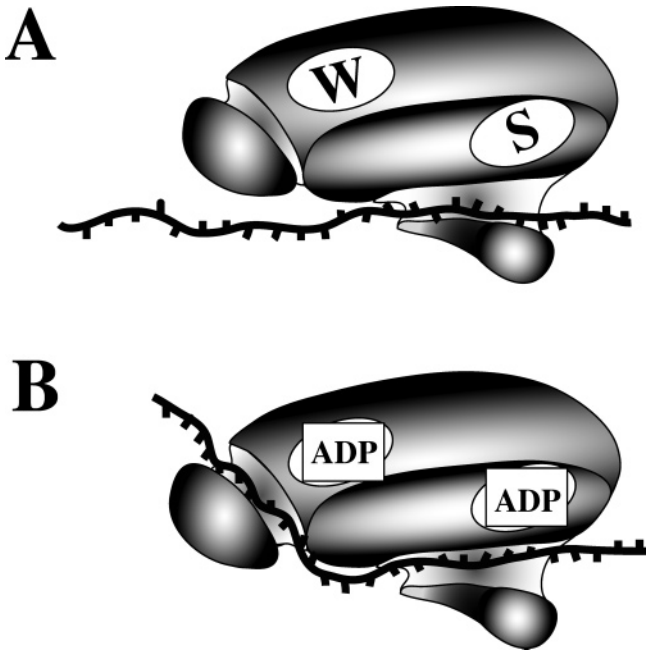

FIGURE 11: Schematic model of the ADP effect on the interactions of the PriA helicase with the ssDNA that encompasses the entire total DNA-binding site of the enzyme, on the basis of the results obtained in this paper. The bound enzyme occludes ~20 nucleotide residues, which is the site size of the total DNA-binding site of the helicase (A) (*18*−*20*). The proper DNA-binding site of the PriA helicase has a site size of ~6 nucleotide residues and is located on a domain that protrudes from the main body of the enzyme. In the absence of nucleotide cofactors in the strong (S) or weak (W) nucleotide-binding site, only the proper DNA-binding site can engage in interactions with the ssDNA (*18*−*20*). The strong nucleotide-binding site, which is the high-affinity ATPase site of the enzyme activated by the bound ssDNA, is presumably located adjacent to the proper DNA-binding site. The additional interacting area of the total DNA-binding site is in a "closed" state and, in the absence of ADP, is not available for the nucleic acid. When ADP occupies both strong and weak binding site of the helicase, the nucleic acid changes its conformational state in the proper DNA-binding site and/or its orientation (B). Moreover, the area of the total DNA-binding site assumes an "open" state and is now capable of engaging in interactions in an additional part of the DNA molecule, now suitably oriented in the proper DNA-binding site and long enough to encompass the total DNA-binding site of the helicase (see the text for details).

by thermodynamic and kinetic studies, the proper DNA-binding site of the PriA helicase that has a site size of 6 ± 1 nucleotide residues is located on a domain that protrudes from the main body of the enzyme (*18*−*20*). In the absence of nucleotide cofactors in the strong (S) or weak (W) nucleotide-binding site or in the presence of nucleoside triphosphate, only the proper DNA-binding site can engage in interactions with the ssDNA (*18*−*20*). The total DNA-binding site of the enzyme has a site size of 20 ± 3 nucleotide residues, which is much larger than the site size of the proper DNA-binding site and includes an additional area that can engage in interactions with the DNA. However, in the absence of ADP, this additional interacting area of the total DNA-binding site is in a "closed" state and is not available for the nucleic acid. When ADP occupies both strong and weak binding sites of the helicase, the nucleic acid changes its conformational state in the proper DNA-binding site and/or its orientation. Moreover, the additional area of the total DNA-binding site assumes an "open" state and is now capable of engaging in interactions in an additional part of the DNA molecule, now suitably oriented in the proper DNA-binding site and long enough to encompass the total DNA-binding site of the helicase (Figure).

Functional Implications. Thus far, the activity of a helicase, particularly, the effect exerted by the nucleotide cofactors on the enzyme affinity for the nucleic acid has been considered in terms of the presence of only a single nucleotide-binding site on the enzyme (*2*−*4*). The discovery of the two nucleotide-binding sites of the PriA helicase dramatically changes the current thinking regarding the nature and the mechanism of interplay between the nucleotide cofactors and the bound nucleic acid in the complex with the helicase. The obtained results provide profound insight into the role of each site in the control of the helicase affinity for the DNA. Such a control by multiple nucleotide-binding sites is a property of the helicase mechanism, which has never been observed before.

As we discussed in refs *46* and *47*, very different energetics, dynamics, and structure of the strong nucleotide-binding site as compared to the weak nucleotide-binding site, as well as a different magnesium effect, argue for different roles of both nucleotide-binding sites in the functioning of the PriA helicase. Although the strong site is the high-affinity ATPase site of the PriA protein, it does not affect the interactions of the helicase with the ssDNA, independent of whether it is associated with ADP or ATP analogues. These results indicate that ATP hydrolysis in the strong site does not affect the enzyme affinity for the ssDNA, unless the weak site is also occupied by an ADP molecule. Thus, the role of ATP hydrolysis in the strong binding site, in controlling the affinity of the enzyme for the nucleic acid, would predominantly serve to exchange ATP for ADP through ATP hydrolysis. On the other hand, the control of the affinity for the DNA by the weak nucleotide-binding site could occur through both the exchange of ATP for ADP and the enzymatic hydrolysis of ATP [ribonucleoside 5′-triphosphate (NTP)] in the site. Therefore, the switch of the PriA helicase between the low- and high-affinity states for the ssDNA, a property that plays a fundamental role in the mechanical translocation along the nucleic acid lattice and unwinding reaction, would rely on the coordinated interplay between the ATP hydrolysis in the strong site and nucleotide exchange and/or ATP hydrolysis in the weak site.

Noticeably, in chromosomal DNA replication, the role of the PriA helicase seems to be related predominantly to the initiation of the restarting of DNA replication after the replication fork stalls, at the damaged DNA sites (*15*, *16*). The enzyme requires short ssDNA gaps to initiate its helicase activity and reassembly of the primosome (*15*, *16*). In other words, the PriA helicase is able to recognize short ssDNA gaps. The optimal length of the recognized ssDNA gap is ~5 nucleotide residues. The helicase can achieve this through its proper DNA-binding site with the site size of 6 ± 1 nucleotide residues, which protrudes from the rest of the protein molecule (*18*−*20*). The data described here indicate that such a searching mode occurs when the two nucleotide-binding sites of the enzyme are free, associated with ATP [NTP or deoxyribonucleoside 5′-triphosphate (dNTP)] or when the weak site is occupied by ADP [NDP or deoxyribonucleoside 5′-diphosphate (dNDP)] and the strong site by ATP (NTP or dNTP). The lack of ATPase or dATPase activity in the absence of DNA indicates that the enzyme is

predominantly in the searching mode in the cell.

The PriA helicase is capable of specifically recognizing the fork structure at the damaged DNA sites (*15*, *16*). Moreover, the helicase specifically recognizes the primosome assembly site (PAS) in the formation of the primosome on phage Φ174 (*8*−*10*). This recognition cannot be achieved through the proper DNA-binding site with the site size of only 6 ± 1 nucleotide residues. However, when both nucleotide-binding sites are saturated with ADP, the total DNA-binding site switches to the open conformation with the efficiency dependent upon the type of base of the cofactor (see above). Thus, the enzyme can engage an additional interaction area of the total DNA-binding site. Although this is not necessary for finding a short ssDNA gap, it would be crucial for the recognition complex structures of the replication fork or the PAS site. The obtained data also explain why the monomeric enzyme that can bind the ssDNA with the site size of 6 ± 1 nucleotide residues has a total DNA-binding site with the site size of 20 ± 3 residues (*18*−*20*). The total DNA-binding site of the PriA helicase switches between the closed and open conformations, under ATP/ADP or dATP/dADP binding and hydrolysis control, allowing the enzyme to engage in interactions with the DNA in an area that is outside of the proper DNA-binding site (Figure 11). In other words, the same mechanism that is involved in the power stroke of the helicase in the translocation and unwinding reaction and relies on the ATP/ADP binding and or hydrolysis in the strong and weak nucleotide-binding sites of the enzyme would be operational in the recognition process of the arrested replication fork structures as well as the PAS site.

ACKNOWLEDGMENT

We thank Betty Sordahl for reading the manuscript.

REFERENCES

1. Kornberg, A., and Baker, T. A. (1992) *DNA Replication*, Freeman, San Francisco, CA, pp 275−293.
2. Lohman, T. M., and Bjornson, K. P. (1996) Mechanisms of helicase-catalyzed DNA unwinding, *Annu. Rev. Biochem. 65*, 169−214.
3. von Hippel, P. H., and Delagoutte, E. (2002) Helicase mechanisms and the coupling of helicases within macromolecular machines. Part I: Structures and properties of isolated helicases, *Q. Rev. Biophys. 35*, 431−478.
4. von Hippel, P. H., and Delagoutte, E. (2003) Helicase mechanisms and the coupling of helicases within macromolecular machines. Part II: Integration of helicases into cellular processes, *Q. Rev. Biophys. 36*, 1−69.
5. Matson, S. W., and Kaiser-Rogers, K. A. (1990) DNA helicases, *Annu. Rev. Biochem. 59*, 289−329.
6. Galletto, R., Jezewska, M. J., and Bujalowski, W. (2004) Unzipping mechanism of the double-stranded DNA unwinding by a hexameric helicase. Quantitative analysis of the rate of the dsDNA unwinding, processivity and kinetic step-size of the *Escherichia coli* DnaB helicase using rapid quench-flow method, *J. Mol. Biol. 343*, 83−99.
7. Galletto, R., Jezewska, M. J., and Bujalowski, W. (2004) Unzipping mechanism of the double-stranded DNA unwinding by a hexameric helicase. The effect of the 3′ arm and the stability of the dsDNA on the unwinding activity of the *Escherichia coli* DnaB helicase, *J. Mol. Biol. 343*, 101−114.
8. Marians, K. J. (1999) PriA: At the crossroads of DNA replication and recombination, *Prog. Nucleic Acid Res. Mol. Biol. 63*, 39−67.
9. Sangler, S. J., and Marians, K. J. (2000) Role of PriA in replication fork reactivation in *Escherichia coli*, *J. Bacteriol. 182*, 9−13.
10. Lee, M. S., and Marians, K. J. (1987) *Escherichia coli* replication factor Y, a component of the primosome, can act as a DNA helicase, *Proc. Natl. Acad. Sci. U.S.A. 84*, 8345−8349.
11. Nurse, P., DiGate, R. J., Zavitz, K. H., and Marians, K. J. (1990) Molecular cloning and DNA sequence analysis of *Escherichia coli* priA, the gene encoding the primosomal protein replication factor Y, *Proc. Natl. Acad. Sci. U.S.A. 87*, 4615−4619.
12. Lee, E. H., Masai, H., Allen, G. C., Jr., and Kornberg, A. (1990) The priA gene encoding the primosomal replicative n′ protein of *Escherichia coli*, *Proc. Natl. Acad. Sci. U.S.A. 87*, 4620−4624.
13. Nurse, P., Liu, J., and Marians, K. J. (1999) Two modes of PriA binding to DNA, *J. Biol. Chem. 274*, 25026−25032.
14. McGlynn, P., Al-Deib, A. A., Liu, J., Marians, K. J., and Lloyd, R. G. (1997) The DNA replication protein PriA and the recombination protein RecG bind D-loops, *J. Mol. Biol. 270*, 212−221.
15. Jones, J. M., and Nakai, H. (1999) Duplex opening by primosome protein PriA for replisome assembly on a recombination intermediate, *J. Mol. Biol. 289*, 503−516.
16. Jones, J. M., and Nakai, H. (2001) *Escherichia coli* PriA helicase: Fork binding orients the helicase to unwind the lagging strand side of arrested replication forks, *J. Mol. Biol. 312*, 935−947.
17. Gorbalenya, A. E., and E. V. Koonin (1993) Helicases: Amino acid sequence comparisons and structure−function relationships, *Curr. Opin. Struct. Biol. 3*, 419−429.
18. Jezewska, M. J., Rajendran, S., and Bujalowski, W. (2000) *Escherichia coli* replicative helicase PriA protein-single-stranded DNA complex. Stoichiometries, free energy of binding, and cooperativities, *J. Biol. Chem. 275*, 27865−27873.
19. Jezewska, M. J., and Bujalowski, W. (2000) Interactions of *Escherichia coli* replicative helicase PriA protein with single-stranded DNA, *Biochemistry 39*, 10454−10467.
20. Galletto, R., Jezewska, M. J., and Bujalowski, W. (2004) Multistep sequential mechanism of *E. coli* helicase PriA protein−ssDNA interactions. Kinetics and energetics of the active ssDNA-searching site of the enzyme, *Biochemistry 43*, 11002−11016.
21. Bujalowski, W., and Jezewska, M. J. (1995) Interactions of *Escherichia coli* primary replicative helicase DnaB protein with single-stranded DNA. The nucleic acid does not wrap around the protein hexamer, *Biochemistry 34*, 8513−8519.
22. Ledneva, R. K., Razjivin, A. P., Kost, A. A., and Bogdanov, A. A. (1978) Interaction of tobacco mosaic virus protein with synthetic polynucleotides containing a fluorescent label: Optical properties of poly(ϵA) and poly(ϵC) copolymers and energy migration from the tryptophan to 1,N^6-ethenoadenine or 3,N^4-ethenocytosine residues in RNP, *Nucleic Acids Res. 5*, 4225−4243.
23. Tolman, G. L., Barrio, J. R., and Leonard, N. J. (1974) Choroacetaldehyde-modified dinucleoside phosphates. Dynamic fluorescence quenching and quenching due to intramolecular complexation, *Biochemistry 13*, 4869−4878.
24. Baker, B. M., Vanderkooi, J., and Kallenbach, N. R. (1978) Base stacking in a fluorescent dinucleoside monophosphate: ϵApϵA, *Biopolymers 17*, 1361−1372.
25. Jezewska, M. J., Kim, U.-S., and Bujalowski, W. (1996) Interactions of *Escherichia coli* primary replicative helicase DnaB protein with nucleotide cofactors, *Biophys. J. 71*, 2075−2086.
26. Jezewska, M. J., and Bujalowski, W. (1997). Quantitative analysis of ligand−macromolecule interactions using differential quenching of the ligand fluorescence to monitor the binding, *Biophys. Chem. 64*, 253−269.
27. Bujalowski, W., and Jezewska, M. J. (2000) *Spectrophotometry and Spectrofluorimetry. A Practical Approach* (Gore, M. G., Ed.) pp 141−165, Oxford University Press, New York.
28. Lohman, T. M., and Bujalowski, W. (1991) Thermodynamic methods for model-independent determination of equilibrium binding isotherms for protein−DNA interactions: Spectroscopic approaches to monitor binding, *Methods Enzymol. 208*, 258−290.
29. Jezewska, M. J., and Bujalowski, W. (1996) A general method of analysis of ligand binding to competing macromolecules using the spectroscopic signal originating from a reference macromolecule. Application to *Escherichia coli* replicative helicase DnaB protein−nucleic acid interactions, *Biochemistry 35*, 2117−2128.
30. Hiratsuka, T. (1983) New ribose-modified fluorescent analogs of adenine and guanine nucleotides available as substrates for various enzymes, *Biochim. Biophys. Acta 742*, 496−508.
31. Turner, D. C., and Brand, L. (1968) Quantitative estimation of protein binding site polarity. Fluorescence of *N*-arylaminonaphthalenesulfonates, *Biochemistry 10*, 3381−3390.

32. Bujalowski, W., and Klonowska, M. M. (1994) Structural characteristics of the nucleotide-binding site of *Escherichia coli* primary replicative helicase DnaB protein. Studies with ribose and base-modified fluorescent nucleotide analogs, *Biochemistry 33*, 4682−4694.
33. Bujalowski, W., and Klonowska, M. M. (1994) Close proximity of tryptophan residues and ATP-binding site in *Escherichia coli* primary replicative helicase DnaB protein. Molecular topography of the enzyme, *J. Biol. Chem. 269*, 31359−31371.
34. Hill, T. L. (1985) *Cooperativity Theory in Biochemistry. Steady State and Equilibrium Systems*, Springer-Verlag, New York, pp 167−234.
35. Jezewska, M. J., Kim, U.-S., and Bujalowski, W. (1996) Binding of *Escherichia coli* primary replicative helicase DnaB protein to single-stranded DNA. Long-range allosteric conformational changes within the protein hexamer, *Biochemistry 35*, 2129−2145.
36. Jezewska, M. J., Rajendran, S., and Bujalowski, W. (1998) Transition between different binding modes in rat DNA polymerase β−ssDNA complexes, *J. Mol. Biol. 284*, 1113−1131.
37. Bujalowski, W., and Jezewska, M. J. (2000) Kinetic mechanism of the single-stranded DNA recognition by *Escherichia coli* replicative helicase DnaB protein. Application of the matrix projection operator technique to analyze stopped-flow kinetics, *J. Mol. Biol. 295*, 831−852.
38. Rajendran, S., Jezewska, M. J., and Bujalowski, W. (2001) Multiple-step kinetic mechanisms of the ssDNA recognition process by human polymerase β in its different ssDNA binding modes, *Biochemistry 40*, 11794−11810,
39. Jezewska, M. J., Rajendran, S., Galletto, R., and Bujalowski, W. (2001) Kinetic mechanisms of rat polymerase β−ssDNA interactions. Quantitative fluorescence stopped-flow analysis of the formation of the (pol β)$_{16}$ and (pol β)$_5$ ssDNA binding mode, *J. Mol. Biol. 313*, 977−1002.
40. Bujalowski, W., Jezewska, M. J., and Galletto, R. (2002) Dynamics of gapped DNA recognition by human polymerase β, *J. Biol. Chem. 277*, 20316−20327.
41. Galletto, R., and Bujalowski, W. (2002) The *E. coli* replication factor DnaC protein exists in two conformations with different nucleotide binding capabilities. I. Determination of the binding mechanism using ATP and ADP fluorescent analogues, *Biochemistry 41*, 8907−8920.
42. Jencks, W. P. (1980) On the attribution and additivity of binding energies, *Proc. Natl. Acad. Sci. U.S.A. 78*, 4046−4050.
43. Jencks, W. P. (1980) The utilization of binding energy in coupled vectorial processes, *Adv. Enzymol. 51*, 75−106.
44. Zavitz, K. H., and Marians, K. J. (1992) ATPase-deficient mutants of the *Escherichia coli* DNA replication protein PriA are capable of catalyzing the assembly of active primosome, *J. Biol. Chem. 267*, 6933−6940.
45. Lee, M. S., and Marians, K. J. (1990) Differential ATP requirements distinguish the DNA translocation and DNA unwinding activities of the *Escherichia coli* PriA protein, *J. Biol. Chem. 265*, 17078−17083.
46. Lucius, A. L., Jezewska, M. J., and Bujalowski, W. (2006) The *Escherichia coli* PriA helicase has two nucleotide-binding sites differing dramatically in their affinities for nucleotide cofactors. 1. Intrinsic affinities, cooperativities, and base specificity of nucleotide cofactor binding, *Biochemistry 45*, 7202−7216.
47. Lucius, A. L., Jezewska, M. J., Roychowdhury, A., and Bujalowski, W. (2006) Kinetic mechanisms of the nucleotide cofactor binding to the strong and weak nucleotide-binding site of the *Escherichia coli* PriA helicase. 2, *Biochemistry 45*, 7217−7236.

BI0518287